Article

Immunity

A pan-family screen of nuclear receptors in immunocytes reveals ligand-dependent inflammasome control

Graphical abstract

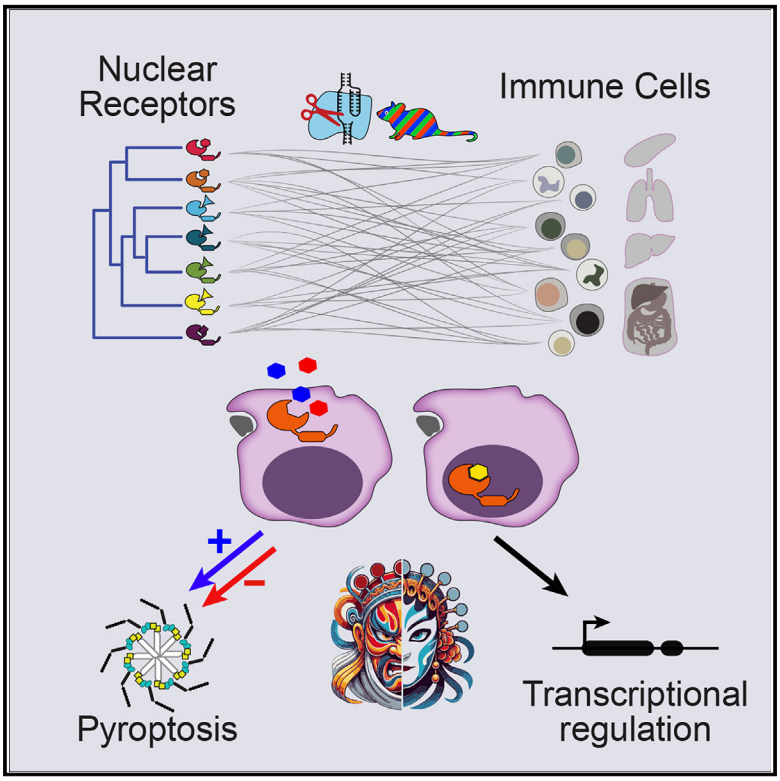

Authors

Yutao Wang, Yanbo Zhang, Kyungsub Kim, ..., Jonathan C. Kagan, Diane Mathis, Christophe Benoist

Correspondence

cbdm@hms.harvard.edu

In brief

Through an *in vivo* Rainbow-CRISPR screen, Wang et al. systematically assess the roles of each of 35 nuclear receptors (NRs) across the immune system, revealing focal, cell-specific involvements as well as noncanonical functions. In cavity macrophages, transcriptional regulation of differentiation by RXRα contrasted with the ligand-dependent activation or inhibition of inflammasome activation by RARγ.

Highlights

- Nuclear receptors have widespread and cell-type-specific roles in immunocytes
- Macrophages residing in different tissues are influenced by distinct retinoid receptors
- RXRα regulates peritoneal macrophage differentiation via chromatin and transcription
- RARγ regulates GATA6^{+} macrophage pyroptosis in a ligand-dependent manner

Wang et al., 2024, Immunity *57*, 1–18
December 10, 2024
https://doi.org/10.1016/j.immuni.2024.10.010

CellPress

Immunity

CellPress

Article

A pan-family screen of nuclear receptors in immunocytes reveals ligand-dependent inflammasome control

Yutao Wang,[1] Yanbo Zhang,[1] Kyungsub Kim,[2] Jichang Han,[3] Daniel Okin,[4] Zhaozhao Jiang,[5] Liang Yang,[1] Arum Subramaniam,[6] Terry K. Means,[6] Frank O. Nestlé,[6] Katherine A. Fitzgerald,[5] Gwendalyn J. Randolph,[3] Cammie F. Lesser,[2] Jonathan C. Kagan,[4] Diane Mathis,[1] and Christophe Benoist[1,7,*]

[1]Department of Immunology, Harvard Medical School, Boston, MA, USA
[2]Center for Bacterial Pathogenesis and Department of Microbiology, Massachusetts General Hospital and Harvard Medical School, Boston, MA, USA
[3]Department of Pathology, Washington University School of Medicine, St. Louis, MO, USA
[4]Division of Gastroenterology, Boston Children's Hospital and Harvard Medical School, Boston, MA, USA
[5]Division of Innate Immunity, Department of Medicine, University of Massachusetts Chan Medical School, Worcester, MA, USA
[6]Immunology and Inflammatory Research Therapeutic Area, Sanofi, Cambridge, MA, USA
[7]Lead contact
*Correspondence: cbdm@hms.harvard.edu
https://doi.org/10.1016/j.immuni.2024.10.010

SUMMARY

Ligand-dependent transcription factors of the nuclear receptor (NR) family regulate diverse aspects of metazoan biology, enabling communications between distant organs via small lipophilic molecules. Here, we examined the impact of each of 35 NRs on differentiation and homeostatic maintenance of all major immunological cell types *in vivo* through a "Rainbow-CRISPR" screen. Receptors for retinoic acid exerted the most frequent cell-specific roles. NR requirements varied for resident macrophages of different tissues. Deletion of either *Rxra* or *Rarg* reduced frequencies of GATA6$^+$ large peritoneal macrophages (LPMs). Retinoid X receptor alpha (RXRα) functioned conventionally by orchestrating LPM differentiation through chromatin and transcriptional regulation, whereas retinoic acid receptor gamma (RARγ) controlled LPM survival by regulating pyroptosis via association with the inflammasome adaptor ASC. RARγ antagonists activated caspases, and RARγ agonists inhibited cell death induced by several inflammasome activators. Our findings provide a broad view of NR function in the immune system and reveal a noncanonical role for a retinoid receptor in modulating inflammasome pathways.

INTRODUCTION

Nuclear receptors (NRs) are a superfamily of ligand-dependent transcription factors, evolutionarily represented in all metazoans.[1] They regulate many aspects of eukaryotic physiology, with the common characteristic of enabling communication between distant cells and organs via small lipophilic molecules.[2–5] First discovered as regulators that underpin endocrine communication between organs through steroid hormones, NRs are now recognized as broader metabolic and toxicological sensors and regulators through their ability to discriminate between small lipid molecules.[6,7] NRs are important pharmacological targets, accounting for 16% of the Food and Drug Administration (FDA)-approved small-molecule drugs.[5,8]

NRs are structurally conserved, sharing two common domains: a DNA-binding domain (DBD) and a C-terminal ligand-binding domain (LBD).[9] Lipophilic substances such as sex steroids, corticoids, or thyroid hormones are endocrine ligands that bind to and activate NRs, whereas others are environmentally derived or modified, like bile acids or retinoids.[6,7] Several NRs are classified as orphans as their ligands remain incompletely determined. Ligand binding induces a conformational change in NRs that enables or strengthens their interaction with specific DNA sequence motifs in promoters and enhancers of their target genes and/or the recruitment of other co-activators and co-repressors.[4,10,11] Steroid-hormone receptors typically bind DNA as monomers or homodimers, but some NRs heterodimerize—in particular, retinoid X receptor (RXR) family members, together with retinoic acid (RA) receptors (RARs), vitamin-D receptor (VDR), and thyroid hormone receptor (THR).[4,12] Heterodimeric RXRs can be activated by RXR ligand (9-*cis*-RA), the partner receptor's ligand, or both, resulting in synergistic outcomes.[3,4]

Classic steroid-hormone receptors (glucocorticoid receptor [GR], ER, PR, and AR) are cytoplasmic and translocate to the nucleus upon ligand binding,[13] where their major modulation of transcription takes place. Several non-genomic actions of NRs and their ligands have also been reported outside the nucleus,

Please cite this article in press as: Wang et al., A pan-family screen of nuclear receptors in immunocytes reveals ligand-dependent inflammasome control, Immunity (2024), https://doi.org/10.1016/j.immuni.2024.10.010

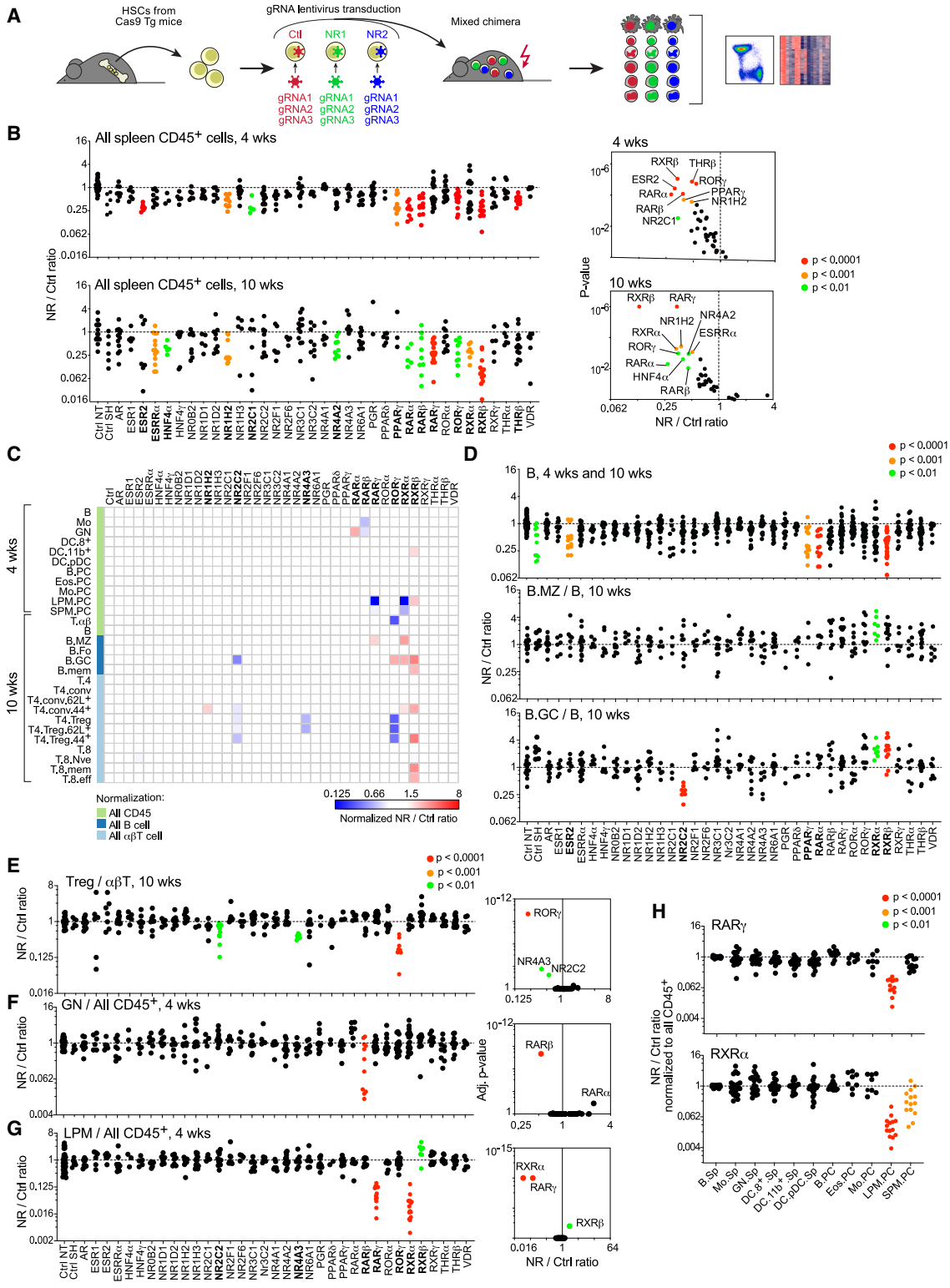

Figure 1. *In vivo* CRISPR screen for roles of nuclear receptors in immunological cell types

(A) Schematic of Rainbow CRISPR screen. Bone marrow stem cells from Cas9 transgenic mice were purified, infected with lentiviruses expressing control or NR-targeting gRNAs, and transferred to lethally irradiated CD45.1 congenic host. Progeny cells in different immunological lineages were analyzed by flow cytometry or gene expression profiling.

(B) Effect of NR inactivation on total donor-derived CD45$^+$ splenocytes. Left: the ratio of frequencies of NR-targeting gRNA vs. control gRNA (NR/Ctrl ratio) of total donor-derived CD45$^+$ cells in the same mouse. "Ctrl NT" derives from control BMC mice that received several non-targeting control gRNAs, similarly measured to

(legend continued on next page)

Please cite this article in press as: Wang et al., A pan-family screen of nuclear receptors in immunocytes reveals ligand-dependent inflammasome control, Immunity (2024), https://doi.org/10.1016/j.immuni.2024.10.010

e.g., interacting with phosphoprotein signaling cascades.[14–17] Furthermore, Nur77 (encoded by *Nr4a1*) has been reported to bind lipopolysaccharide (LPS) and cytoplasmic double-stranded DNA (dsDNA) and activates the NLRP3 inflammasome.[18] Non-genomic signaling occurs on a much faster timescale than transcriptional modulation.

Some NRs are known to play important functions in the immune system. Most classically, corticosteroids acting via NR3C1 (GR) are anti-inflammatory.[19] RORγ is essential for lymphoid organogenesis and innate lymphoid cell or T cell differentiation.[20–25] NR4A receptors regulate T regulatory (Treg) differentiation in the thymus and control T cell activation.[26,27] RA, a group of vitamin A metabolites acting through receptors of the RAR and RXR subfamilies, impacts a number of lymphoid or myeloid cell types[28–35] and stem cells.[36] Even some "metabolic" NRs have been implicated in the function of particular immunocytes, like PPARγ in adipose-tissue Treg cells[37] or LXRβ in activated T cells.[38] But most of these are disparate observations, and there is no comprehensive perspective on the immunological function of the 35 NR family members that are expressed in mouse innate or adaptive immunocytes.

Here, we performed an *in vivo* "Rainbow-CRISPR" screen to investigate the effect of NRs on the differentiation and homeostatic maintenance of all major immunological cell types. CRISPR targeting was performed in hematopoietic stem cells (HSCs), followed by reconstitution of all immunological compartments. Both widespread and cell-type-specific effects were observed—in particular those involving RARs. Mechanistic exploration pinpointed instances of classic control of differentiation via DNA binding and transcription but also a wholly unexpected control of programmed cell death (PCD) pathways, positive or negative according to bound ligands. These findings provide a broad landscape of NR action and a novel conceptual framework for the transcriptional and inflammasome-mediated regulation of cell fate by RA.

RESULTS

In vivo Rainbow-CRISPR screen of homeostatic roles of NRs in the immune system

We set up an *in vivo* Rainbow-CRISPR screen to comprehensively investigate how the NR family affects the differentiation and homeostatic maintenance of immunologic cell types (Figure 1A). We targeted all 35 NR genes expressed in at least some immunocytes (Figure S1A, ImmGen data). CRISPR editing was achieved by infecting HSCs from Cas9-expressing mice with gRNA expressing lentiviral vectors. The cells were then used to reconstitute all immunologic lineages of lethally irradiated recipients (Figure 1A). In the Rainbow strategy, each bone marrow chimera (BMC) mouse is internally controlled, receiving a mix of three HSC populations, each identifiable with different fluorescent reporters: two are transduced with lentiviruses targeting a given gene and one with a non-targeting control (Table S1A in practice, each targeting actually pooled 3 different gRNAs against the same gene, coded with the same fluorescent reporter). This configuration enabled a direct comparison of wild-type (WT) and mutant cells differentiated in the same environment. In addition, to guard against an effect of the double-stranded breaks created in the HSCs, we used gRNAs inducing breaks in "safe harbor" loci. After allowing reconstitution and differentiation to proceed (4 weeks for myeloid cells, 10 weeks for lymphocytes), the effect of NR inactivation was assessed by flow cytometry as the relative abundance of progeny cells identified by the three fluorescent reporters in each of 28 innate or adaptive immunocytes (gating strategies in Figures S1B–S1E). This strategy was preferred to sequencing-based identification as it required far fewer cells for robust quantification and hence was better adapted to assay small cell subsets. Editing efficacy was verified by amplicon sequencing around the gRNA target sites in both the HSC population prior to transfer and in recovered B lymphocytes. Only a few gRNAs seemed ineffective, with 37%–97% (95% interval) of chromosomes showing a mutation for each gRNA (median 68%; Figure S1F; Table S1C). Given that each targeting involved 3 independent gRNAs, we infer that 41%–99% of HSCs (median 81%) carried homozygous deletion mutations of the target gene (with the exception of *Nr4a1*).

To uncover broad effects at the level of HSCs, we first analyzed the relative proportions of total CD45$^+$ donor-derived cells derived from NR- or control-targeted HSCs within the same mouse. The results (Figure 1B; Table S1D) denoted several impacts of NR ablation on these pan-lineage readouts, although some NRs appeared neutral (ESR1, NR2F6, or THRα; note, however, a trend toward lower frequencies of cells carrying safe-harbor gRNAs, suggesting a slight effect of double-stranded breaks in HSCs on later differentiation). We surmise that these frequent reductions reflect, at least in part, the pleiotropic roles of many NRs in HSCs.[36]

We then addressed our primary goal, the role of NRs in differentiated immunocytes, factoring out fluctuations in global reconstitution efficiency by normalizing frequencies of edited progeny

estimate experimental variance. "Ctrl SH" represents the control gRNAs that target safe harbor genome locations. Right: volcano plots showing the summary data for the mean NR/Ctrl ratio differentially changed by NR ablation.

(C) Summary of screen results, all NRs, and cell types. Average NR/Ctrl ratios of donor-derived immunological cell types, normalized to NR/Ctrl ratios of whole donor-derived CD45$^+$ cells or whole spleen B or whole spleen αβT cells, as indicated. Only cells with $|FC| > 1.5$ and adj.$p < 0.05$ are color coded. Global changes in total B cells are not discernible because they constitute a substantial fraction of CD45$^+$ cells, causing effects to disappear when normalized to donor-derived CD45$^+$ cells.

(D) Effect of NR ablations on B cells (total, B.MZ, and B.GC). Dot plots of NR/Ctrl ratios as in (B), normalized to NR/Ctrl ratios of total B cell for B.MZ and B.GC.

(E–G) Effect of NR ablations, dot plots of NR/Ctrl ratios for spleen Tregs normalized to all αβT cells (E), neutrophils (GN, F), and large peritoneal macrophages (LPMs, G) normalized to donor-derived CD45$^+$ splenocytes, corresponding volcano plots at right.

(H) NR/Ctrl ratios for RARγ and RXRα ablations in different myeloid cell types from spleen and peritoneum, normalized to donor-derived CD45$^+$ splenocytes.

Each dot is an individual mouse. Significance was assessed using one-sample t test in (B), (D top), and (H); one-way ANOVA with Dunnett correction in (D, bottom rows) and (E)–(G). Only NR mutants with fold-change $|FC| > 2$, nominal $p < 0.01$ are color coded as indicated: $p < 0.0001$ is shown in red, $p < 0.001$ in orange, and $p < 0.01$ in green.

See also Figures S1 and S2 and Table S1.

Please cite this article in press as: Wang et al., A pan-family screen of nuclear receptors in immunocytes reveals ligand-dependent inflammasome control, Immunity (2024), https://doi.org/10.1016/j.immuni.2024.10.010

in each cell type against relative frequencies in total edited CD45$^+$ cells in the same mouse host. Overall, a number of NR involvements were detected where the deletion of one or several NRs led to increased or decreased proportions of specific immunocytes, as portrayed in Figure 1C (detailed in Figures 1D–1H and S2A–S2F; Tables S1E and S1F). Among the most noteworthy:

(1) B cells as a whole were affected by the deletion of several NRs (Figure 1D, top), with the strongest dependence on RXRβ, RARα, and PPARγ. Narrowing in on the more differentiated states showed that mutation of these same NRs relatively increased marginal zone (MZ) and germinal center (GC) B cell differentiation (Figures 1D lower rows, S2A, and S2B), consistent with the complex positive and negative roles of retinoids in B cells.[39] In contrast, the requirement for the orphan receptor NR2C2 was more specific to B.GC cells.

(2) Within αβT lymphocytes (Figures S2C and S2D), RORγ had the strongest impact, which was a positive control of sorts given the known requirement for RORγ in immature double-positive pre-T cells.[20] We also noted the more modest effects of NR4A3 and of NR1H2 (LXRβ) on the abundance of αβT cells in the spleen (Figure S2D), aligning with their well-established functions in thymic T cell differentiation.[38,40] We saw no apparent impact of LXRβ ablation on Treg proportions and T cell activation (Figure S2E).

(3) In Treg cells (Figures1E and S2F), RORγ deletion elicited an unexpected drop of FoxP3$^+$ Treg cells, which was not merely due to the general dearth of T cells because the results were normalized against total αβT cells. We also identified the effects of NR4A3, in line with the reported roles of NR4A family members in Tregs, although somewhat unexpected given the reported redundancy among NR4A family members.[26,27] The NR2C2 deficiency also marginally affected Treg numbers (Figure S2F).

(4) In granulocytes, previous studies have shown that RARα functions as a bidirectional regulator of neutrophil differentiation.[41] Here, RARα appeared to be a negative regulator of spleen neutrophils but RARβ seemed to positively influence their numbers (Figure 1F).

(5) Peritoneal macrophages (MFs) showed the strongest effect of any deletion, with the very deep (10- to 30-fold) decrease in large peritoneal MFs (LPMs) after elimination of either RARγ or RXRα (Figure 1G). Elimination of RXRα also impacted the population of small peritoneal MFs (SPMs) that arise and maintain distinctly from LPMs. This effect was specific in that no other myeloid lineage was similarly affected (Figure 1H). In contrast to SPMs, LPMs are known to be influenced by RA and its derivatives,[29,42] and the present data anchor this relationship through mechanisms that will be detailed below.

This screen thus provided a broad perspective on the roles of NRs in the differentiation and homeostasis of various innate and adaptive cell types. As a class, the RARs were the most often involved, in keeping with the pleiotropic actions of RA in the immune system.[43] Other NRs, those binding specific hormone families, were less frequently implicated—surprisingly including NR3C1 (GR), the conduit for major anti-inflammatory compounds, which showed no detectable effect on levels of any cell type.

Transcriptional profiling of NR deficiencies in LPMs

For a mechanistic understanding of these effects, we focused on the MFs that manifested the strongest effects in the screen. We performed gene expression profiling to better understand the very similar consequences of RXRα and RARγ ablation on LPM numbers and to identify other NRs expressed in LPMs that might influence their phenotypes but not their numbers. Therefore, NR-deficient peritoneal MFs (CD11b^{hi}F4/80^{hi}) purified from BMC mice 4 weeks after reconstitution were used for low-input RNA sequencing (RNA-seq)[44] (Figures 2A and 2B; Table S2). Perhaps surprisingly, most NRs showed little effect (Figure 2A), with only mild imprints by NR1H3 and NR2C2 deficiencies (we are unsure of the NR2C2-related fold changes [FCs], because the cluster of genes affected reproducibly by NR2C2 ablation had high inter-replicate variability in samples with ablation of other NRs, suggesting non-specific noise). But RXRα and RARγ mutants dominated these changes, with two major gene clusters upregulated or downregulated in concert by the two mutations and two smaller clusters more strongly affected by RXRα deficiency (also evidenced in the FC/FC plots of Figure 2C). These dominant clusters included genes overexpressed in LPMs relative to other MFs in previous studies[29,45,46] and from our single-cell RNA-seq (scRNA-seq) data (per below) and genes activated or repressed by GATA6, as deduced from previous ablation studies[29,47,48] (Figure 2B, right). *Gata6* itself was downregulated in both RXRα- and RARγ-deficient MFs (Figure 2C). These effects fit with the loss of LPMs in response to RXRα or RARγ deficiency (Figures 1G and 1H), which would proportionally increase in SPMs, but also pointed to quantitative variations between the two.

Tissue-resident MFs influenced by RA through distinct RA receptors

RXRα and RARγ deficiencies appeared to have very similar consequences on peritoneal MFs, in line with vitamin A's role in regulating LPM identity[29] and with RXR's importance in serous cavity MFs.[30] We asked whether the strong dependence on RXRα and RARγ was a general property of all MFs. Tissue-resident MFs (TRMs) vary across organs and adapt to unique microenvironments, exemplified by alveolar MFs in the lung and Kupffer cells in the liver.[15,49–51] LPMs belong to the "cavity MF" category, contributing to rapid responses to barrier breach or organ damage.[52–54] All TRMs express RA receptors, albeit with different patterns[55] (Figure S3A), and virtually all were affected by the RA deficiency caused by a vitamin-A-deficient diet (Figure S3B), expanding on previous reports.[29,56,57] Prompted by these results, we extended the CRISPR screen to systematically assess in Rainbow BMC mice the impact of RA receptors on different donor-derived TRMs, including MFs that infiltrate the transplanted MC38 tumors (Figures 3A and 3B; Table S3; gating strategies in Figure S3C). The deep impact of RARγ deficiency was unique to LPMs, whereas the loss of RXRα impacted most other TRM populations, except colon or visceral adipose tissue (VAT) MFs, in line with previous

Please cite this article in press as: Wang et al., A pan-family screen of nuclear receptors in immunocytes reveals ligand-dependent inflammasome control, Immunity (2024), https://doi.org/10.1016/j.immuni.2024.10.010

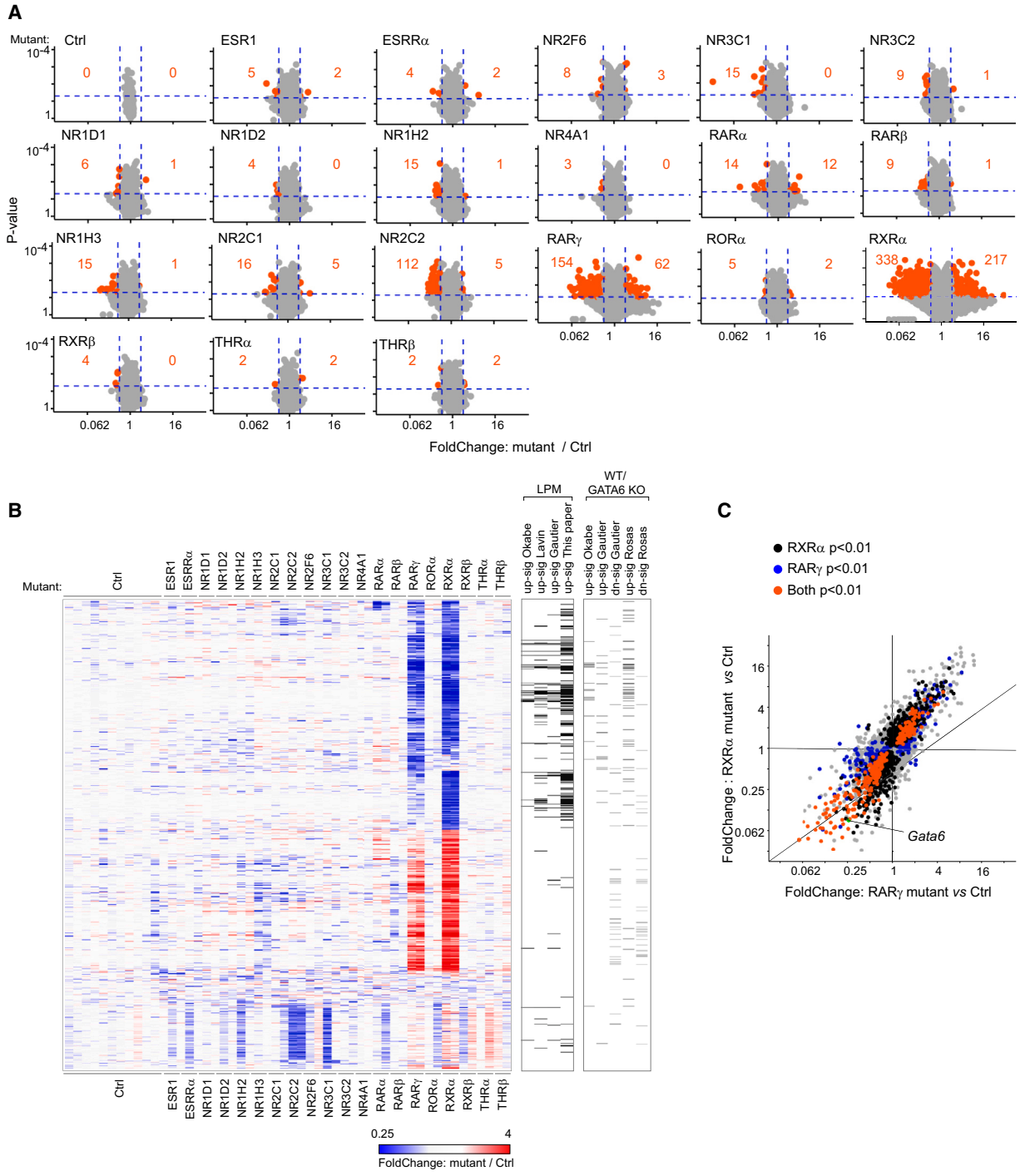

Figure 2. Transcriptional consequences of NR deficiencies in peritoneal macrophages

Bulk RNA-seq was performed in biological duplicates on donor-derived peritoneal MFs of Rainbow-CRISPR mice with deficiencies in LPM-expressed NRs.

(A) Volcano plots showing genes differentially expressed in NR mutant vs. non-targeting gRNA controls, and one pair of held-back controls. Number of transcripts with |FC| > 2 and nominal $p < 0.05$ are shown.

(B) Heatmap grouping differentially expressed genes (|FC| > 2 and nominal $p < 0.05$ in any one deficiency). All profiling in biological duplicate, both shown. Row annotations at right show signatures of gene overexpressed in LPM,[29,45,46] and GATA6-regulated genes[29,47,48] (see Table S2).

(C) FC/FC plots relating changes elicited by RXRα and RARγ deficiencies in LPMs. Transcripts meeting nominal $p < 0.01$ in one or both mutants are highlighted. Significance was assessed using one-sample t test in (A).

See also Table S2.

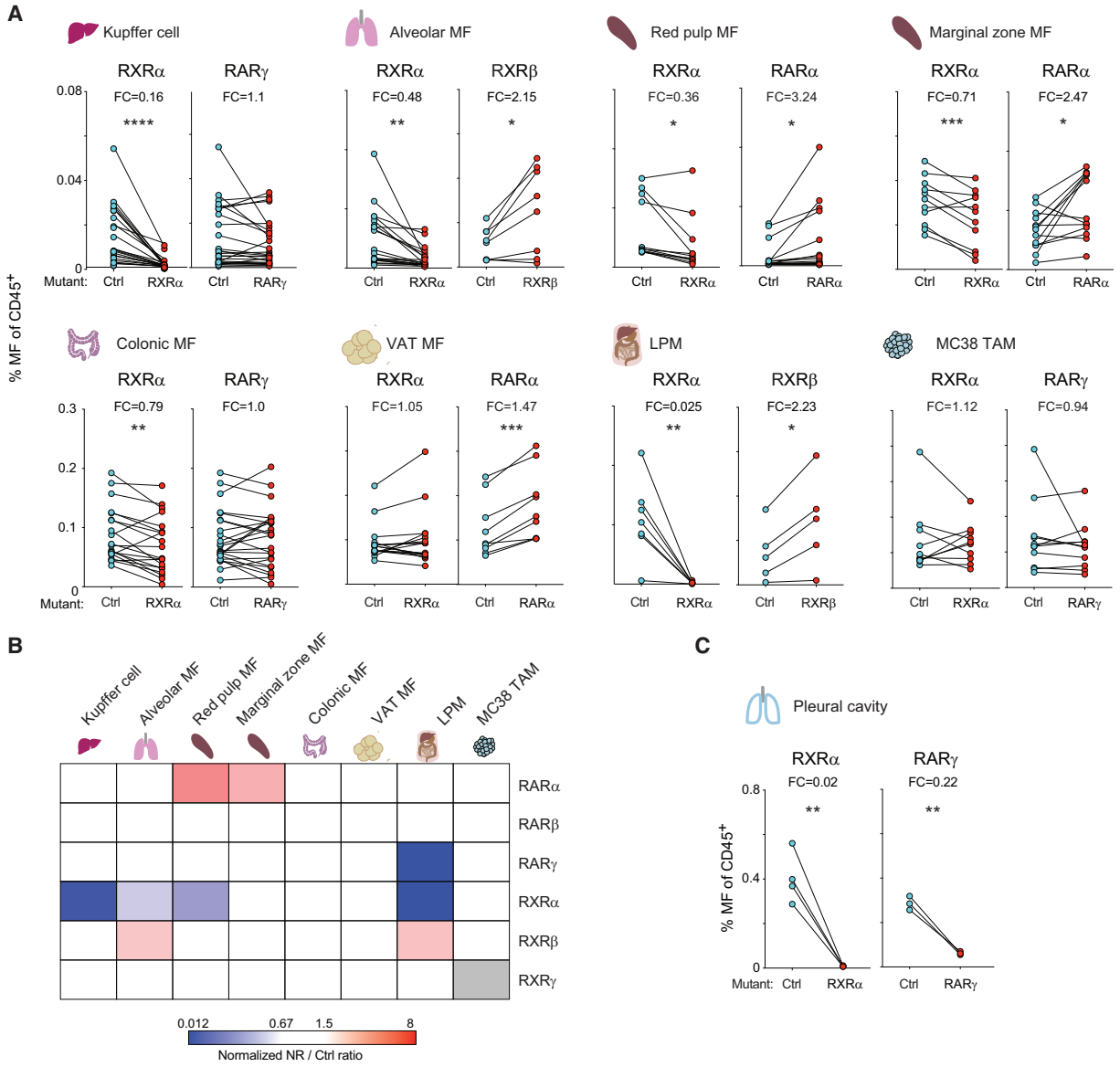

Figure 3. Tissue-resident macrophages are influenced by distinct RA receptors

Tissue-resident and tumor-infiltrating macrophages were analyzed in Rainbow-CRISPR mice with deficiencies in all RA receptors, 4–5 weeks after reconstitution.

(A) Proportion of MFs carrying illustrative control or NR-targeting gRNAs within total donor-derived CD45$^+$ cells in each tissue, measured by flow cytometry. Each pair from an individual mouse. FC values (mutant/Ctrl) are shown. $n > 5$.

(B) Heatmap summarizing the NR/Ctrl ratios in TRMs and MC38 TAMs, normalized to NR/Ctrl ratios of total donor-derived CD45$^+$ cells in each tissue, color-coded only where $|FC| > 1.5$ and nominal $p < 0.05$. Gray: insufficient data.

(C) As in (A), proportions of pleural cavity MFs carrying control and RXRα- or RARγ-targeting gRNAs within total donor-derived CD45$^+$ cells. $n = 3–4$.

Significance was assessed using paired t test. *$p < 0.05$, **$p < 0.01$; ***$p < 0.001$; ****$p < 0.0001$.

See also Figure S3 and Table S3.

reports that RXRα governs the differentiation of yolk sac or erythromyeloid progenitor-derived TRMs.[58] Generally, the data revealed a patchwork of dependencies that varied between TRMs (Figure 3B). RARβ and RXRγ were not required by any TRMs, although RARα and RXRβ appeared to have inhibitory effects on several TRMs, again with a different distribution (RXRβ most inhibitory to alveolar MFs, RARα to red pulp MFs). Thus, RA controls the differentiation and homeostasis of TRMs through distinct receptors.

GATA6$^+$ MFs with similar transcriptional identities are found in serous cavities like peritoneal, pleural, and pericardial spaces.[52] To verify whether the unique dependency on RARγ applied to the GATA6$^+$ MF class more generally, we analyzed GATA6$^+$ MFs in the pleural cavity of BMC mice repopulated with RARγ- and RXRα-deficient HSCs (Figure 3C). The same deep drop was observed as in LPMs, indicating that this unique dual dependency is a general property of GATA6$^+$-cavity MFs.

Please cite this article in press as: Wang et al., A pan-family screen of nuclear receptors in immunocytes reveals ligand-dependent inflammasome control, Immunity (2024), https://doi.org/10.1016/j.immuni.2024.10.010

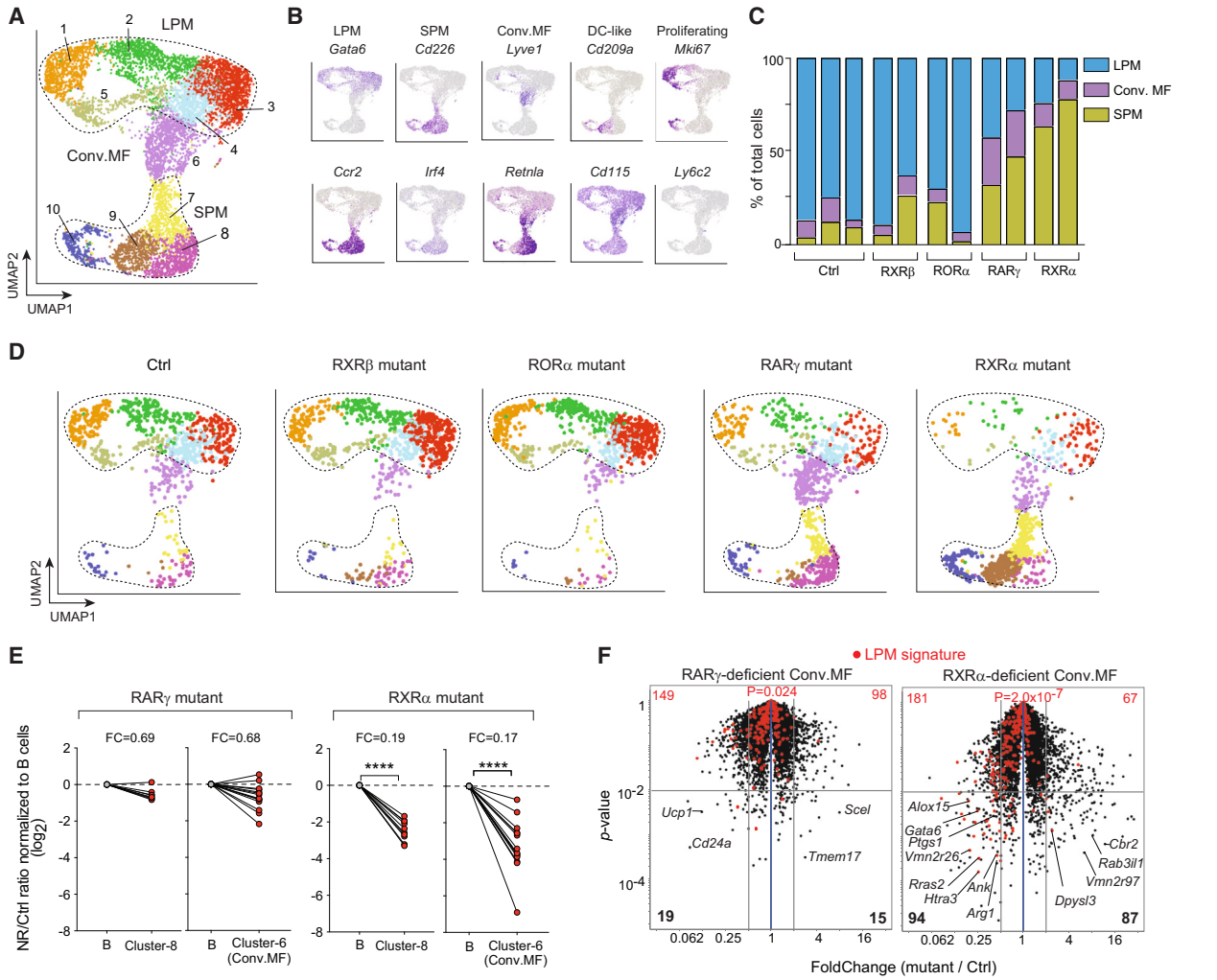

Figure 4. RXRα and RARγ control LPMs in distinct ways

Multiplex scRNA-seq analysis of CD11b$^+$CD115$^+$ peritoneal cells from Rainbow-CRISPR mice with deficiencies in several RA receptors, 17 days after reconstitution.

(A) UMAP projection of the whole data, color-coded by Louvain clustering. Clusters annotated as LPM or SPM delineated by dotted lines.

(B) As in (A), color-coded by expression of key genes that define the MF populations shown.

(C) Proportions of LPM, SPM, and converting MF within total CD11b$^+$CD115$^+$ cells. Each bar is an individual sample.

(D) Individual UMAP plots of Ctrl, RXRβ mutant, RORα mutant, RARγ mutant, and RXRα mutant cells. All groups were downsampled to an equal number of cells for comparison.

(E) Flow cytometric analysis of the equivalents of clusters 6 and 8 (gating strategy per Figure S4D), shown as dot plots of NR/Ctrl ratios for RARγ and RXRα ablations, normalized to frequencies in peritoneal B cells of the same mice. n = 8–14.

(F) Conv. MFs from Ctrl, RARγ-, or RXRα-deficient BMCs were profiled by population RNA-seq. The volcano plots show differential expression (mutant/Ctrl), with counts of transcripts passing |FC| > 2 and p < 0.01 shown at the bottom. LPM signature transcripts[46] are highlighted in red (significance of the imbalance estimated by chi-squared test).

See also Figure S4 and Table S4.

RXRα and RARγ control LPMs in different ways

To examine more closely the varied effects of RA receptor deletions on peritoneal MFs and determine whether inactivation of RXRα and RARγ elicited superimposable effects on different LPM clusters (as predicted if they operate as a heterodimer, a known propensity of RXR proteins[3]), we performed scRNA-seq analyses on total CD11b$^+$CD115$^+$ peritoneal cells from BMC mice edited for several RA receptors, 17 days after reconstitution (each in biological duplicate and all multiplexed by hashtagging into the same run for optimal comparability[59]). As shown in Figure 4A, uniform manifold approximation and projection (UMAP) and Louvain clustering identified 10 cell clusters within CD11b$^+$CD115$^+$ cells that could be categorized into LPM (GATA6$^+$F4/80^{hi}, clusters 1–5) and SPM (CD226$^+$IRF4$^+$, clusters 7–10), and also distinguished a LYVE1$^+$CD206$^+$ cluster-6 with transcriptional characteristics intermediate between LPM and SPM, which is often annotated as "converting MFs"[60,61] (Figures 4B, S4A, and S4B). Transfer of these LYVE1$^+$CD206$^+$

Please cite this article in press as: Wang et al., A pan-family screen of nuclear receptors in immunocytes reveals ligand-dependent inflammasome control, Immunity (2024), https://doi.org/10.1016/j.immuni.2024.10.010

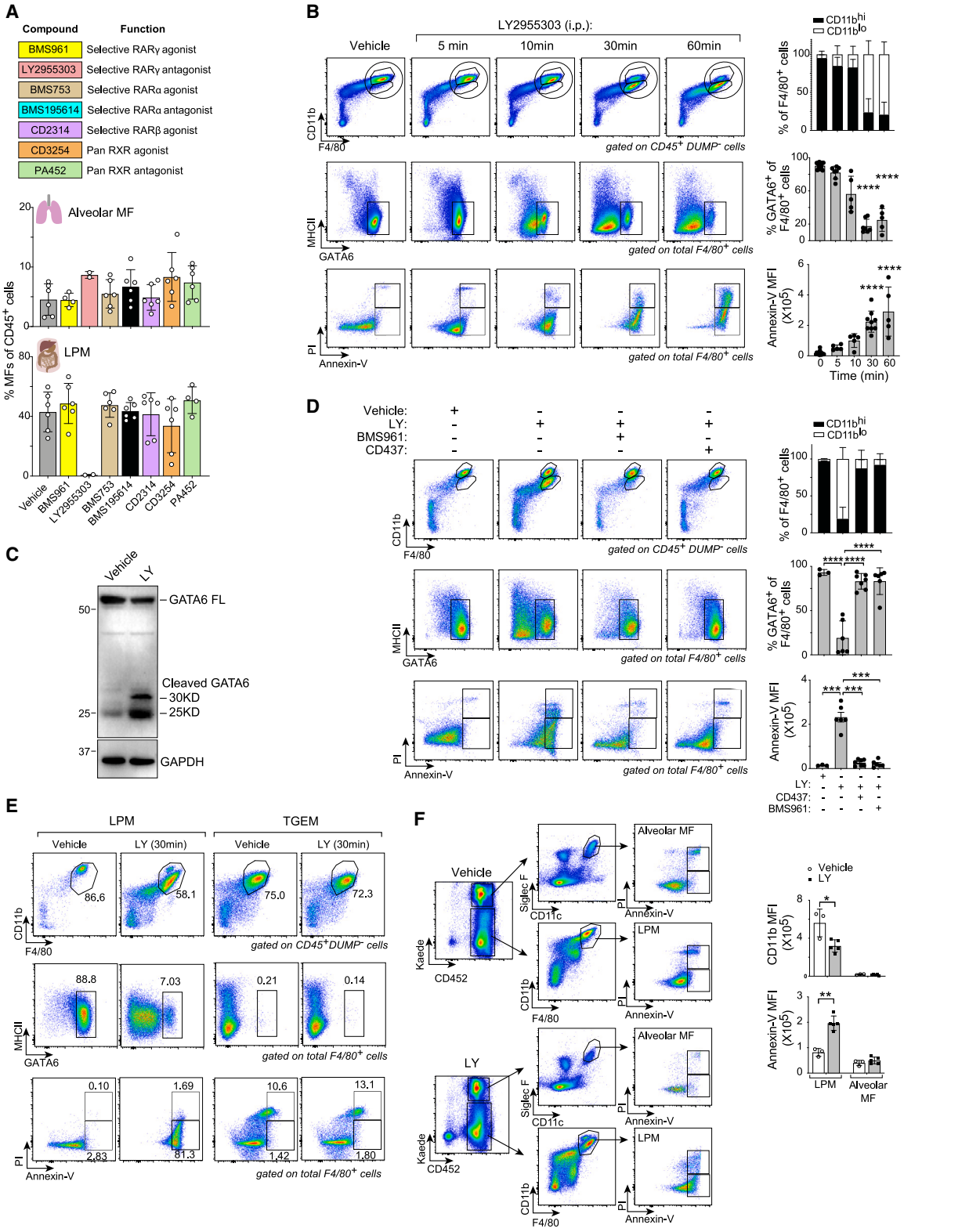

Figure 5. RARγ antagonist induces rapid loss of GATA6 and cell death in LPMs

Agonist and antagonist compounds that affect RA receptors were injected i.p. into B6 mice and the effects evaluated by flow cytometry.

(A) Compounds used (see Table S6), and proportions of alveolar macrophages and LPMs after 6 days (injection every other day), $n = 2–6$.

(legend continued on next page)

cells confirmed that they are indeed LPM precursors. Cells with either RORα or RXRβ deficiencies yielded largely the same distribution as WT MFs (Figure 4C), with essentially identical cluster frequencies (Figure 4D represents equal numbers of cells from each condition and Figure S4C shows the same maps downsampled to match actual numbers of deficient CD11b$^+$CD115$^+$ cells). Deficiencies in RARγ and RXRα both caused a marked decrease in LPM clusters, as expected (Figures 4C, 4D, and S4C). Sequencing of the gRNA target regions in LPMs that remain in spite of RARγ or RXRα deficiencies showed them enriched in unmutated loci. However, these two deficiencies differed in the distributions of SPM and precursor clusters (Figure 4D): RARγ-deficient cells appeared similar to those of WT (with an apparent increase in cluster-6 and -8 due to the loss of LPMs); RXRα-deficient cells showed a strong reduction in cluster-6 and -8, with a corresponding increase in SPM cluster-9, which expresses higher levels of dendritic cell (DC)-associated CD209a, consistent with the possibility that loss of RXRα favored the more DC-like orientation of SPMs described previously.[62–64] These differences were verified by flow cytometric analysis of BMC mice with these deficiencies (Figure 4E; gating strategies in Figure S4D). Thus, the RARγ deficiency allowed entry of precursors into the peritoneal cavity, and some differentiation into cluster-6 cells thereafter, whereas the RXRα deficiency entailed more immediate perturbations. It is interesting to note that the distribution of RARγ-deficient peritoneal MFs (very few GATA6$^+$ LPM and many LYVE1$^+$) resembles that found in human peritoneal cavity MFs,[61] an observation that may be connected to the low levels of RARγ in human cells.

To evaluate the transcriptional consequences of the two mutations independently of the LPM loss that dominated the bulk profiles of Figure 2, we analyzed differentially expressed genes (DEGs) by RNA-seq profiling of sorted LYVE1$^+$CD206$^+$ MFs (cluster-6 equivalent) from WT and mutant cells (Figure 4F; Tables S4B and S4C). The RARγ deficiency had little impact (only 15 and 19 genes upregulated and downregulated at arbitrary cutoffs ($|FC| > 2$ and $p < 0.01$), not very different from experimental noise in such experiments. The loss of RXRα had more severe consequences (181 affected genes altogether). Interestingly, the expression of *Alox15*, *Ltc4s*, and *Ptgs1*, which encode key enzymes controlling conversion of arachidonic acid (AA) to cysteinyl leukotrienes and prostaglandins, was specifically downregulated in RXRα, but not in RARγ mutants (Figures 4F and S4G), hinting that AA metabolites might influence LPM maturation.[65] We also analyzed patterns of genomic DNA binding by chromatin immunoprecipitation (ChIPmentation[66]). Peaks of significant binding were observed in whole peritoneal MFs of WT mice with anti-RXRα (n = 876) (Figure S4E; Table S5A), but we could not obtain convincing data with anti-RARγ. RXRα-binding peaks were significantly enriched ($p < 10^{-100}$) in NR-binding motifs, notably those for RARs (Figure S4F). A significant proportion of these peaks mapped in the vicinity (defined as closest gene, mostly within 30 kb) of genes positively controlled by RXRα in peritoneal MFs (Figure S4G; Table S5B). Taken together, these results showed that, although they both controlled LPM numbers, RARγ and RXRα did so in a different manner: RXRα acted as a classical TF, binding and transactivating the expression of genes that are essential for LPM differentiation. In contrast, RARγ allowed normal maturation of the precursors, its absence having only limited transcriptional impact and its importance becoming apparent only at the mature LPM stage.

RARγ antagonist induces rapid loss of GATA6 and death in LPMs

To orthogonally validate our genetic data, we used a panel of synthetic agonists and antagonists to modulate the activity of RA receptors in WT mice *in vivo* (intraperitoneal [i.p.] injection over a week), assessing the effect on LPMs and lung alveolar MFs. In keeping with the genetic screen, the selective RARγ antagonist LY2955303 (hereafter "LY") dramatically reduced LPM frequency but had no effect on lung alveolar MFs (Figure 5A). Compounds targeting RXRα or other NRs had no such effect.

We then used this specific inhibitor for mechanistic investigations of the control of LPMs by RARγ. We quickly realized that LY's action on LPMs was extremely rapid: several manifestations appearing within 10 min, much faster than could be accounted for by transcriptional changes (Figure 5B). CD11b and F4/80 were down-modulated from the surface of LPMs and GATA6 levels were even more dramatically reduced, with evidence of proteolytic cleavage (Figure 5C); plasma membranes exhibited evidence of PCD, as revealed by annexin-V and propidium iodide (PI) staining (Figure 5B). These effects were also observed in recipients of transfers of reporter-tagged LPMs, indicating that they reflected true modifications of LPMs rather than rapid recruitment of other cells into the peritoneum (Figure S5A). At later time points (3 h after LY injection), an influx of monocytes and neutrophils into the peritoneal cavity indicated the pro-inflammatory nature of these events.

Several points argued that these outcomes denoted true biology as opposed to simple toxicity or off-target action. First,

(B) Flow cytometric time-course plots of CD11b vs. F4/80 expression (top), and GATA6 vs. major histocompatibility complex (MHC)-II (middle) or annexin-V vs. propidium iodide binding (bottom) within total F4/80$^+$ cells, after i.p. injection of vehicle or 50 nmol LY. Left: representative staining profiles; right: summary data. n = 5–9.

(C) Immunoblot analysis of GATA6 protein in whole-cell lysates of total peritoneal cells, 10 min after i.p. injection of vehicle or 50 nmol LY.

(D) Flow cytometric analysis as in (B) from mice treated with RARγ agonists (30 nmol BMS961, 15 nmol CD437) before LY treatment for 20 min. n = 3–7.

(E) Flow cytometric analysis as in (B) from mice pretreated with 3% thioglycolate 2 days previously to induce thioglycolate-elicited macrophages (TGEMs), before LY treatment for 30 min.

(F) Lung alveolar CD45$^+$ cells purified from Kaede reporter mice were transferred into the peritoneum of normal B6 hosts; vehicle or LY was injected 10 min later, and peritoneal cells harvested 30 min later for flow cytometry as in (B). Detection of the Kaede reporter (left) allowed the parsing of endogenous LPM (Kaede$^-$) vs. transferred alveolar MFs (Kaede$^+$). n = 3–5.

DUMP$^-$ means CD3$^-$CD19$^-$Ly6C$^-$Ly6G$^-$ cells. Representative of 3 experiments in (C) and (E). Mean ± SD. Significance was assessed using one-way ANOVA in (B) and (D) and t test in (F). p values as per Figure 3.

See also Figure S5 and Table S6.

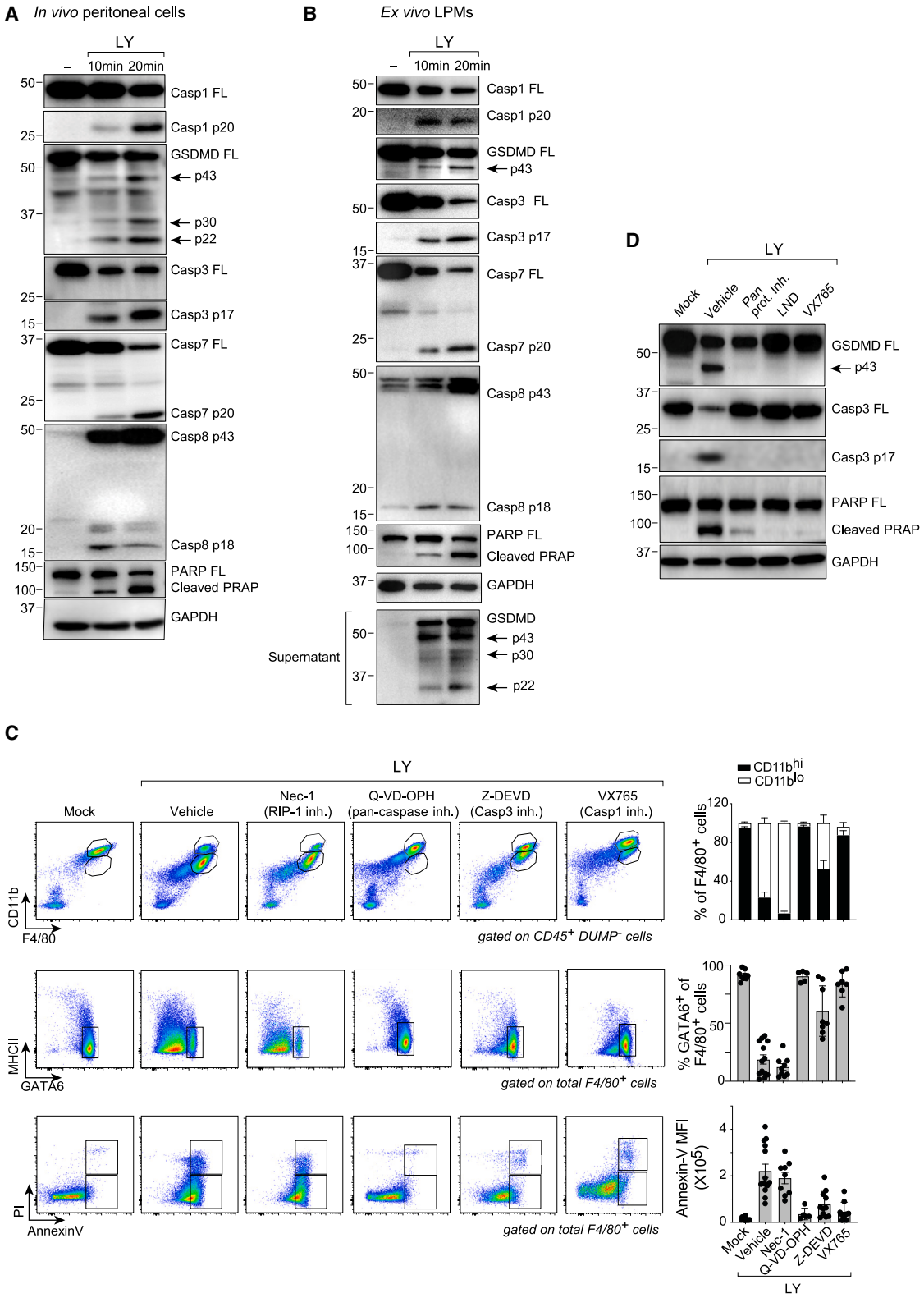

Figure 6. RARγ antagonist activates a caspase-1-dependent programmed cell death

(A and B) Immunoblot analysis of PCD signaling in lysates of peritoneal cells isolated from vehicle- or 50 nmol LY-injected B6 mice (A) or in both lysates and supernatants from purified LPMs left untreated or treated with 50 μM LY (B) for the indicated times (antibodies listed in Table S7).

(legend continued on next page)

they were also observed upon treatment with an independent RARγ antagonist, MM11253 (Figure S5B). Second, LY treatment did not induce notable reductions in the numbers or viability of other peritoneal cell types, including SPMs, B cells, and eosinophils (Figure S5C). Third, and most direct, the effects of LY treatment were hindered by prior administration of the RARγ agonists CD437[67] and BMS961,[68] indicating that the antagonist's impact was specifically reversed by a matching agonist ligand (Figure 5D; the agonists had no discernible effects on their own in this assay). Interestingly, the dose range of LY effectiveness was very sharp, with a transition from virtually no effect (30 nmoles) to full effect (50 nmoles) over a 2-fold span (Figure S5D). LPMs are known to disappear rapidly after triggering of innate receptors by LPS or live bacteria, by migration to the omentum or aggregation on the peritoneal wall within fibrin clots.[29,69,70] However, i.p. injection of LPS did not induce the same downregulation of CD11b and GATA6 as RARγ antagonists did (Figure S5E), indicating that the latter did not simply mimic the actions of innate immune agonists. In sum, these findings demonstrated the highly specific effects of antagonizing RARγ on LPMs.

Because SPM seemed resistant to LY treatment, we investigated target cell specificity in more depth. Thioglycolate-elicited peritoneal MFs, which are GATA6-negative and express lower levels of RARγ, were resistant to LY injection (Figure 5E). Similarly, alveolar MFs and Kupffer cells were not affected by the i.p. administration of LY that perturbed LPMs (Figure S5F). To rule out a compound diffusion problem, and for a direct comparison of MF sensitivity in the same *in vivo* environment, we transferred total lung CD45$^+$ cells from Kaede reporter mice into the peritoneal cavity of naive hosts, followed rapidly by i.p. LY injection. MFs of alveolar origin were still resistant to LY treatment, in a location where endogenous LPMs were fully susceptible (Figure 5F).

This tight specificity for GATA6$^+$ MFs of the RARγ antagonist, coupled with the rapid degradation of GATA6 itself, prompted the hypothesis that GATA6 might participate in LY-induced events. We thus tested the effects of LY administration in mice with cell-specific deficiencies in GATA6 (*Gata6*$^{flox/flox}$ crossed to *LyzM-cre* or *Cd115-creERT2*). Indeed, GATA6 deficiency conferred resistance to LY-induced cell death and a partial effect on CD11b cleavage (Figure S5G).

RARγ antagonist activates a caspase-1-dependent PCD

Proteolytic cleavage of CD11b is associated with neutrophil detachment during chemotaxis.[71] Together with the cleavage of GATA6 described above (Figure 5C) and the speed of events, these observations suggested that LY-induced modifications were initiated by proteolysis rather than by transcriptional modifications. Indeed, injection of a pan-protease inhibitor prior to LY administration resulted in a complete blockage of CD11b, GATA6 downregulation, and annexin-V binding (Figure S6A).

The rapidity of the events induced by antagonism of RARγ, their sensitivity to pan-protease blockade, and the annexin-V binding induced on LPMs suggested the possible involvement of PCD cascades. We therefore evaluated the activation of several molecular players associated with apoptosis, pyroptosis, or necroptosis. Immunoblotting revealed the activation of these pathways in peritoneal cells in the first 20 min after LY injection *in vivo* (Figure 6A), involving molecules associated with several types of PCD. Related to pyroptosis were the cleavage of caspase-1 and the appearance of the active p30 form of gasdermin D (GSDMD), the pyroptosis effector required for membrane pore formation.[72] Related to apoptosis were the cleavage of caspases-3, -7, and -8 and nuclear poly (ADP-ribose) polymerase (PARP) (Figure 6A). Similar proteolytic activation was also induced by LY in purified LPMs in culture, denoting a direct effect of the antagonist (Figure 6B).

Although PCD types were originally defined as independent and segregated processes, it is now recognized that there is significant crosstalk and bridges between them,[73–76] and the multiple cleavages induced by the RARγ antagonist likely reflected such spreading. To identify the key initiators, we injected several PCD inhibitors prior to LY treatment. Inhibition of RIPK1, a key node of necroptosis, had no effect on the various aspects of LY-induced response in LPMs, whereas inhibitors of caspase-1 or caspase-3 effectively blocked all manifestations, as did a pan-caspase inhibitor (Figure 6C). Furthermore, the inhibition of caspase-1 prevented LY-induced cleavage of caspase-3, PARP, and GSDMD (Figure 6D), suggesting that caspase-1, the main driver of canonical pyroptosis, is positioned upstream in the cascade and that RARγ is connected to inflammasome activation.

RARγ inhibits inflammasome activation in a ligand-dependent manner through ASC binding

The main caspase-1 inflammasomes (NLRP1, NLRP3, AIM2, and NLRC4) sense different pathogenic structures or stress-associated stimuli to induce pyroptosis. Most are strictly dependent on the ASC bridging adaptor, except for NLRP1.[77] To test the hypothesis that RARγ regulates inflammasome activation in a ligand-dependent manner, we treated LPMs with the BMS961 (selective RARγ agonist and RA mimic[68] that inhibited LY-induced effects in LPM above) prior to exposure to ligands that canonically activate different inflammasomes: (1) for NLRP3, LPS + ATP, or LPS + nigericin; (2) for AIM2 and poly (dA:dT); and (3) for NLRC4 and *Shigella flexneri*.[78] Indeed, as evidenced by caspase-1 cleavage (Figure 7A) and interleukin (IL)-1β secretion (Figure 7B), the RARγ agonist strongly inhibited caspase-1 activation downstream of all of these inflammasomes, indicating that properly liganded RARγ was able to dominantly block the effects of all these pyroptosis-inducing agents. These results suggested that RARγ antagonists and agonists operate reciprocally, respectively activating or inhibiting

(C) Flow cytometric analysis as in Figure 5B, from mice pretreated with the indicated protease inhibitors (Table S6) for 1 h before i.p. LY injection for 30 min. n = 8–13. DUMP$^-$ means CD3$^-$CD19$^-$Ly6C$^-$Ly6G$^-$ cells.

(D) Immunoblot analysis of lysates from purified LPMs were pretreated or not with 2 μg/μL pan protease inhibitor, 200 μM Ionidamine (LND, ASC inhibitor) or 25 μM VX765 for 1 h and then stimulated with 50 μM LY for 20 min.

See also Figure S6 and Tables S6 and S7.

Please cite this article in press as: Wang et al., A pan-family screen of nuclear receptors in immunocytes reveals ligand-dependent inflammasome control, Immunity (2024), https://doi.org/10.1016/j.immuni.2024.10.010

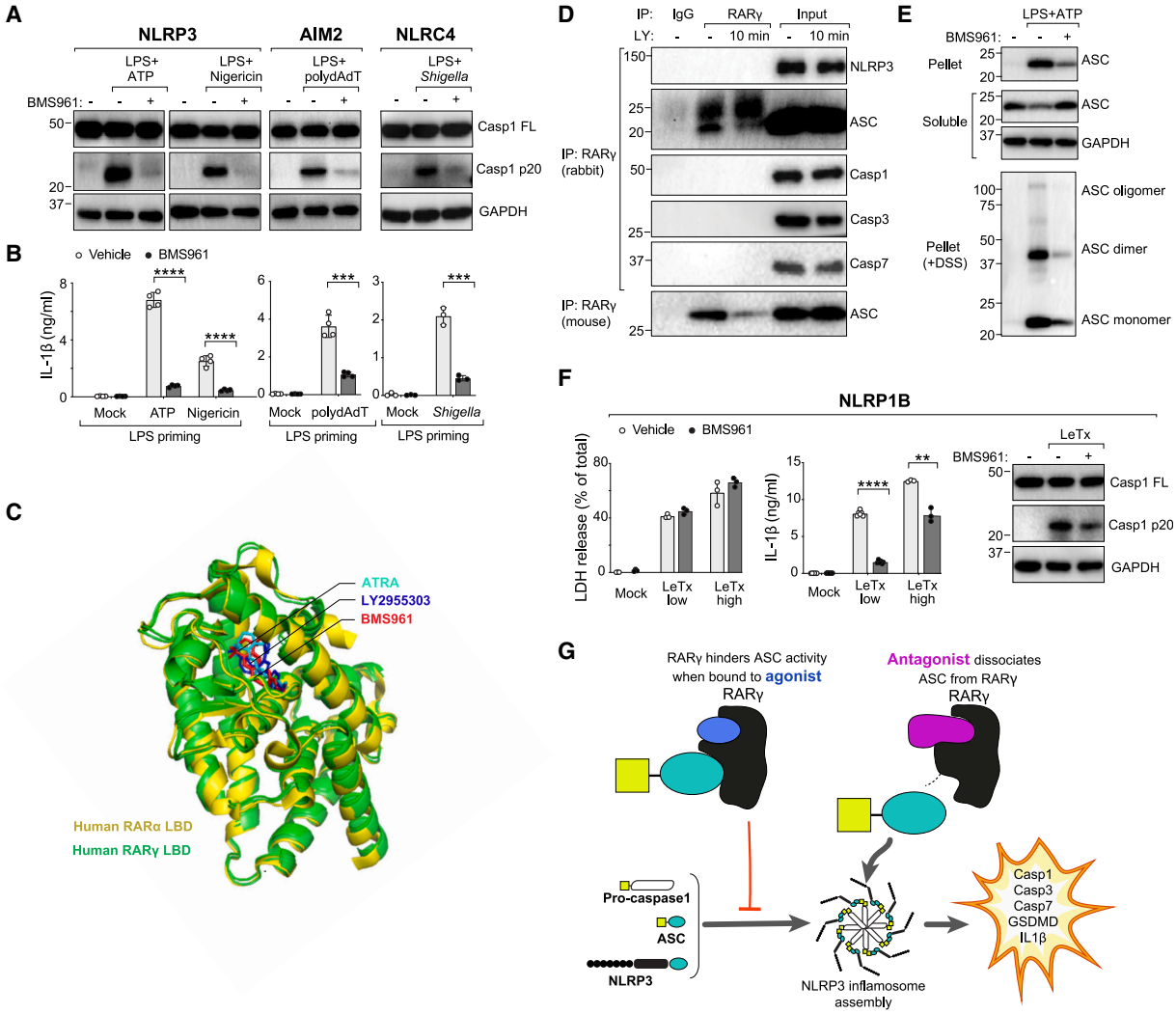

Figure 7. RARγ inhibits inflammasome activation in a ligand-dependent manner through ASC binding

(A and B) Inflammasome activation in the presence of RARγ agonist. LPS-primed primary LPM cells were pretreated or not with 30 μM BMS961 for 1 h *in vitro*, followed by 5 mM ATP or 10 mM nigericin treatment for 30 min, or 2 μg poly(dA:dT) transfection for 6 h, or *Shigella* infection (MOI = 30) for 2 h. Immunoblot analysis of both cell extracts and supernatants (A), and IL-1β assay of supernatants (B). The inflammasome pathway activated by these treatments is shown at top.

(C) Binding of RA, BMS961, and LY2955303 in the ligand-binding pocket of RA receptors (from Klaholz et al.,[68] Renaud et al.,[79] and Hughes et al.[80]). Crystal structures of human RARγ LBD bound to RA (all-*trans*, PDB: 2LBD) or BMS961(PDB: 4LBD), and of human RARα LBD bound to LY2955303 (PDB: 5K13) are superimposed.

(D) Co-immunoprecipitation assay. Several inflammasome components or downstream caspase protease proteins were pulled down with anti-RARγ (two different antibodies) from lysates of peritoneal cells, previously i.p. injected with vehicle or 50 nmol LY for 10 min.

(E) Immunoblot analysis for ASC oligomers in the pellet and soluble fractions of lysates from LPS-primed LPMs that were pretreated or not with 30 μM BMS961 for 1 h, followed by 5 mM ATP treatment for 30 min, without (top) or with (bottom) disuccinimidyl suberate (DSS) cross-linking.

(F) Effect of RARγ agonist on NLRP1 inflammasome activation. BALB/c LPMs were pretreated or not with 30 μM BMS961 for 1 h, prior to exposure to different concentrations of LeTx (low dose, 2 μg/mL protective antigen [PA] + 1 μg/mL lethal factor [LF]) or (high dose,10 μg/mL PA + 10 μg/mL LF) for another 3 h. LDH assay (left) and IL-1β assay (middle) of supernatants, immunoblot analysis of both cell extracts and supernatants (right).

(G) Working model of RARγ in regulation of inflammasome assembly and activation, in a ligand-dependent manner.

Representative of immunoblotting results from three experiments.

Mean ± SD; significance was assessed using t test in (B) and (F). *p* values as per Figure 3.

inflammasome activation. Accordingly, examination of published structures of human RAR bound to these compounds[68,79,80] (Figure 7C) showed that they both associate with the RA-binding pockets of the receptors.

We also performed loss-of-function experiments by examining the effects of the RARγ antagonist LY in *Nlrp3*$^{-/-}$, *Asc*$^{-/-}$, *Casp1*$^{-/-}$*11*$^{-/-}$, and *Gsdmd*$^{-/-}$ mice. In contrast to the strong blockade elicited by chemical inhibitors (in particular of caspase-1 inhibitor), there were only minor differences in LY-induced manifestations in LPMs from these mice (Figure S6B), likely due to the redundancy and compensation in cell death pathways.[73,74,81]

Please cite this article in press as: Wang et al., A pan-family screen of nuclear receptors in immunocytes reveals ligand-dependent inflammasome control, Immunity (2024), https://doi.org/10.1016/j.immuni.2024.10.010

To establish how RARγ interacted with inflammasome complexes, we conducted co-immunoprecipitation experiments, pulling down protein complexes with anti-RARγ antibodies. There was no detectable interaction of RARγ with caspase-1, -3, or -7, or with NLRP3, but a clear binding to ASC, the key adaptor protein of inflammasome assembly and activation, was observed with two independent anti-RARγ Abs (Figure 7D). The interaction between RARγ and ASC was further confirmed by immunoprecipitation of lysates from transfected HEK293T cells (Figure S7A). Notably, LY treatment reduced the interaction between RARγ and ASC, indicating that their interaction was affected by the ligand bound to RARγ (Figure 7D). Consistent with its interaction with ASC, cell fractionation showed that RARγ was not solely nuclear, a sizable fraction being cytoplasmic[17] (Figure S7B). The involvement of ASC was also supported by the observation that pretreatment with the ASC inhibitor lonidamine[82] blocked LY-induced caspase-3 and GSDMD activation in LPMs (Figure 6D) as well as CD11b and GATA6 cleavage (Figure S7C). Oligomerization of ASC is a key feature of inflammasome activation, eliciting downstream caspase recruitment.[83] Further establishing the connection between RARγ and ASC, the agonist BMS691 inhibited the recruitment of ASC into a polymeric insoluble form (Figure 7E, top) and its polymerization (Figure 7E, bottom) by NLRP3 inflammasome inducers.

Should PCD cascades be connected to RARγ and its ligands through ASC, one would predict a different effect of the RARγ agonist on NLRP1-induced pyroptosis, which is considered as ASC independent. The involvement of ASC in NLRP1b inflammasome activation is complex. Although ASC is not required for pyroptosis induced by anthrax lethal toxin (LeTx), the classic NLRP1b activator, it is necessary for caspase-1 autoproteolysis and partially required for IL-1β secretion.[84,85] We treated NLRP1b-expressing LPMs from BALB/c mice with BMS961 prior to LeTx treatment. The agonist indeed had no effect on LeTx-induced cell death, as evidenced by lactate dehydrogenase (LDH) release (Figure 7F). It did partially inhibit IL-1β release, depending on the dose of initiating LeTx, and inhibited caspase-1 autoproteolysis (Figure 7F). This disconnect between readouts mirrors what has been reported for LeTx-activated NLRP1b in ASC-deficient mice,[84] and this parallel strengthens the conclusion that RARγ interferes with ASC activity in a ligand-dependent manner.

Thus, these results demonstrated that RA receptors strongly regulate the LPM population but in very different ways. RXRα does it in a conventional manner, as a transcriptional regulator of genes important for LPM differentiation over time. RARγ, on the other hand, acts on a much faster timescale, as a ligand-dependent rheostat of inflammasome assembly, either facilitating or hindering it in a ligand-dependent manner (Figure 7G).

DISCUSSION

NRs play diverse roles in the immune system, but a comprehensive understanding of how they regulate immunocyte biology was lacking. The *in vivo* screen strategy was applied to systematically determine the influence of 35 murine NRs on the differentiation and homeostatic maintenance of most immunologic cell types, revealing a broad overall effect on repopulation potential as well as some more focused cell-type-specific requirements. Of the latter, the most striking was the impact of RXRα and RARγ deficiencies on GATA6$^+$ LPMs, which occurred through distinct regulatory mechanisms. This exploration revealed an unexpected function of RARγ, which acts in a ligand-dependent manner to either facilitate or dampen an explosive program of proteomic alteration and cell death.

The Rainbow-CRISPR screen uncovered several known and unrecognized functions of NRs in the immune system. Inactivation of many of the NRs mildly affected overall reconstitution frequencies, manifested only as trends for many, suggesting roles in the genetic regulatory network of HSCs and progenitors (such broad effects might also take place in differentiated cell types but were not captured here because they were factored out by the normalization). Of the specific effects, some were unexpected, such as that of the orphan NR2C2 (a.k.a. TR4[86]), with no previously known relationship to B.GC or Treg physiology, whereas others amplified prior knowledge. Consistent with its well-established functions in thymic T cell differentiation, we found that RORγ inactivation impacted αβT cells but, less expectedly, also reduced the fraction of FoxP3$^+$ Treg cells. It remains to be determined whether RORγ regulates thymic Treg differentiation or homeostasis in the spleen. In contrast, inactivation of NR3C1, the receptor for strongly immunoregulatory glucocorticoids, had surprisingly little effect. Overall, perturbing receptors for RA had the most frequent impact, with both positive and negative effects that denote balancing roles in some cells (e.g., RXRα and RARα in red pulp MFs). Some RA receptors affected a whole lineage or differentiated subsets thereof. For instance, total B cells were affected by deletion of RXRβ and RARα, whereas differentiated MZ and GC B cell states were regulated by RXRα and RXRβ. The study also highlighted the diverse influences of RXRα on tissue MF differentiation, consistent with the enrichment of enhancer-bound RXRα protein in TRMs of several origins.[58] Our study, which relied on HSC-differentiated MFs, showed marked divergence between tissues in the requirement for RXRα, prompting the speculation that these differences are due to inductive effects within the tissues but not to the stem cell of origin. PPARγ and LXRα control the functional specification of alveolar and splenic MFs, respectively.[87–89] Because RXRα can heterodimerize with PPARγ and LXRα, it may function paired with them in various TRMs.

From one viewpoint, one might be surprised by the relative paucity of specific effects unearthed in this screen, which was particularly striking in the gene expression profiles of mutant peritoneal MFs. Aside from the dominant effects of RXRα and RARγ deficiencies, most deletions left very subtle or no traces in LPM transcriptomes. One interpretation may be that differentiating cells adjust to the missing NR through functional redundancy between NRs or through more complex adaptations of the genetic regulatory network. In addition, some effects may have been missed because inactivation was not complete or because the cells were only exposed to physiological amounts of hormones or NR ligands and were not specifically challenged or triggered.

The mechanistic exploration revealed the two-pronged transcriptional and inflammasome-mediated regulation of LPM fate, orchestrated by RXRα and RARγ, likely accounting for their previously reported dependence of LPMs on RA.[29,42] LPMs play critical roles in maintaining the integrity of body cavities and have been suggested to be evolutionarily ancient cell types.[52,54] They

Please cite this article in press as: Wang et al., A pan-family screen of nuclear receptors in immunocytes reveals ligand-dependent inflammasome control, Immunity (2024), https://doi.org/10.1016/j.immuni.2024.10.010

are implicated in several diseases, such as postsurgical adhesions, endometriosis, and some cancers. Our genomic analyses demonstrated that RXRα directly controls LPM differentiation through classic transcriptional regulation, consistent with prior studies.[30] Intriguingly, RXRα-controlled genes included several that encode key enzymes in the arachidonic acid pathways, whose metabolites can influence LPM differentiation and phenotype.[65]

Far less expected was the ligand-dependent control of inflammasome activation in LPMs, anchored by the interaction of RARγ with ASC. There are classic precedents for control of cell survival/death by NRs (GR, RORγ, and RAR) through transcriptional modulation of pro- or anti-apoptotic protein expression like Bcl-2 family members or Fas/FasL.[20,90,91] More relevant are recently described instances of cell death affected by NR via non-genomic routes. During tumor necrosis factor (TNF)-induced death, RARγ favors RIP1 dissociation from TNFR1 to form death-signaling complexes.[17] Most recently, NR4A1 has been reported to activate the NLRP3 inflammasome after binding LPS and cytoplasmic dsDNA.[18] Here, RARγ acts as a key checkpoint for LPM survival, flipping between pro- and anti-survival modes. We speculate that agonist and antagonist molecules, which fit the same ligand-binding pocket as RA, result in allosterically distinct RARγ structure. When bound to BMS961 or RA, RARγ binds ASC and supports LPM survival by hindering inflammasome activation by canonical stimuli. Conversely, when bound to its antagonist LY, RARγ dissociates from ASC, which then oligomerizes and provokes a caspase-1-dependent activation of other caspases and gasdermin. It seems unlikely that the agonist-dependent switch in ASC interaction alters a simple stoichiometric sequestering of ASC, and we suspect that a more complex regulation must be at play, in keeping with the highly non-linear "tipping point" mode of inflammasome activation. For instance, the RARγ-ASC complex might interfere with ASC polymerization as a dominant negative. In terms of physiological relevance, this mechanism may allow a finely tuned homeostatic control on LPM populations as a function of RA concentration in serous cavities.[29] Alternatively, or in addition, natural antagonists may exist (endogenous or produced by microbes) that destabilize MF populations, possibly in situations when it is important to rapidly remove MFs from the local cavities. RARγ's influence is tightly restricted to GATA6$^+$ MFs, across body locations or in the LPM maturation cascade. Indeed, GATA6 itself appears to be a player in the phenomenon, as indicated by the reduced sensitivity of GATA6-deficient MFs, in line with reports that GATA6 deficiency renders LPMs more vulnerable to apoptosis and downregulation of CD11b.[47,48] More generally, it will be interesting to see whether regulation of inflammasomes applies to other contexts in which NRs have been associated with cell survival.

Starting from a broad unsupervised survey, this study ended up identifying a striking mode of ligand-regulated control of inflammasome activation, opening the door to explorations of wider involvement of this process in NR function and to potential therapeutic applications.

Limitations of the study

This investigation focused on the role of NRs in immunological homeostasis at steady state in the presence of physiologically supplied ligands. NR functions specific to challenged contexts (inflammation, infection, and tumors) would have been missed. Because the lentivirus-mediated gene inactivations were not complete, we cannot rule out that, in some instances, homeostatic drive might have led to the selective amplification of the unedited fraction of cells (as clearly happens for RXRα-deficient LPMs), masking deeper effects. This situation precluded testing the effect of RARγ-modulating ligands in mature LPMs. Absence of effects should be interpreted with caution, as redundancy between NRs may mask true involvement.

RESOURCE AVAILABILITY

Lead contact

Further information and requests for resources and reagents should be directed to and will be fulfilled by the lead contact, Prof. Christophe Benoist (cbdm@hms.harvard.edu).

Materials availability

This study did not generate new unique reagents.

Data and code availability

Bulk RNA-seq data, scRNA-seq data, and ChIPmentation data generated in this project have been deposited in the Gene Expression Omnibus (GEO) database under accession number GSE254573. Tabulated underlying data for Figures 1, 2, 3, 4, S2, and S4 are available in Tables S1, S2, S3, S4, and S5. External datasets were retrieved from GEO (population RNA-seq for all major immunological cell types from GSE100738, 12 different MF populations from Sequence Read Archive [SRA] PRJNA482293, MC38-tumor-associated MFs from GSE185591, and assay for transposase-accessible chromatin with sequencing [ATAC-seq] data of peritoneal MFs from GSE63338). All other data needed to evaluate the conclusions in the paper are present in the paper or the supplemental information.

ACKNOWLEDGMENTS

We thank V. Piekarsa, K. Hattori, A. Ortiz-Lopez, F. Chen, A. Baysov, J. Lee, I. Magill, C. Araneo, and M. Sleeper for help with viruses, mice, processing, and sorting; N. Patel and D. Mallah for computational help; and P. Chambon, W. Krezel, N. Ghyselinck, H. Gronenmeyer, D. Duteil. P. Germain, and R. Vance for discussions, advice, and reagents. This work was supported by NIH grant RO1-AI150686 and a sponsored research agreement from Sanofi-Genzyme to C.B. and D.M.; RO1-AI169795 to C.F.L.; AI167993, AI116550, and DK34854 to J.C.K.; NIH R37 AI049653 to G.J.R.; T32HL116275 to D.O.; and NIH K00CA264434 to J.H.

AUTHOR CONTRIBUTIONS

Y.W., Y.Z., K.K., and J.H. performed experiments. Y.W., K.K., J.H., and L.Y. analyzed and interpreted data. Y.W. and C.B. wrote the manuscript, which all authors reviewed. D.O., Z.J., A.S., T.K.M., and F.O.N. provided discussions, mice, or funding. C.B., D.M., C.F.L., K.A.F., J.C.K., and G.J.R. provided supervision and acquired funding.

DECLARATION OF INTERESTS

The authors declare no competing interests.

STAR★METHODS

Detailed methods are provided in the online version of this paper and include the following:

- KEY RESOURCES TABLE
- METHOD DETAILS

- Mice
- Cell isolation and flow cytometry
- Rainbow-CRISPR screen
- Population (ULI) RNA-seq
- scRNA-seq analysis of peritoneal macrophages
- Chromatin immunoprecipitation (ChIPmentation)
- *In vitro* cell treatments
- Immunoblotting and protein analysis
- Statistical analyses

- ACCESSION NUMBERS

SUPPLEMENTAL INFORMATION

Supplemental information can be found online at https://doi.org/10.1016/j.immuni.2024.10.010.

Received: February 28, 2024
Revised: July 31, 2024
Accepted: October 23, 2024
Published: November 20, 2024

REFERENCES

1. Bertrand, S., Brunet, F.G., Escriva, H., Parmentier, G., Laudet, V., and Robinson-Rechavi, M. (2004). Evolutionary genomics of nuclear receptors: from twenty-five ancestral genes to derived endocrine systems. Mol. Biol. Evol. *21*, 1923–1937.
2. Mangelsdorf, D.J., Thummel, C., Beato, M., Herrlich, P., Schütz, G., Umesono, K., Blumberg, B., Kastner, P., Mark, M., Chambon, P., et al. (1995). The nuclear receptor superfamily: the second decade. Cell *83*, 835–839.
3. Evans, R.M., and Mangelsdorf, D.J. (2014). Nuclear receptors, RXR, and the big bang. Cell *157*, 255–266.
4. Gronemeyer, H., Gustafsson, J.A., and Laudet, V. (2004). Principles for modulation of the nuclear receptor superfamily. Nat. Rev. Drug Discov. *3*, 950–964.
5. Lazar, M.A. (2017). Maturing of the nuclear receptor family. J. Clin. Invest. *127*, 1123–1125.
6. Kojetin, D.J., and Burris, T.P. (2013). Small molecule modulation of nuclear receptor conformational dynamics: implications for function and drug discovery. Mol. Pharmacol. *83*, 1–8.
7. Sladek, F.M. (2011). What are nuclear receptor ligands? Mol. Cell. Endocrinol. *334*, 3–13.
8. Lonard, D.M., and O'Malley, B.W. (2012). Nuclear receptor coregulators: modulators of pathology and therapeutic targets. Nat. Rev. Endocrinol. *8*, 598–604.
9. Bain, D.L., Heneghan, A.F., Connaghan-Jones, K.D., and Miura, M.T. (2007). Nuclear receptor structure: implications for function. Annu. Rev. Physiol. *69*, 201–220.
10. McKenna, N.J., and O'Malley, B.W. (2002). Combinatorial control of gene expression by nuclear receptors and coregulators. Cell *108*, 465–474.
11. Glass, C.K., and Saijo, K. (2010). Nuclear receptor transrepression pathways that regulate inflammation in macrophages and T cells. Nat. Rev. Immunol. *10*, 365–376.
12. De Bosscher, K., Desmet, S.J., Clarisse, D., Estébanez-Perpiña, E., and Brunsveld, L. (2020). Nuclear receptor crosstalk - defining the mechanisms for therapeutic innovation. Nat. Rev. Endocrinol. *16*, 363–377.
13. Kumar, S., Saradhi, M., Chaturvedi, N.K., and Tyagi, R.K. (2006). Intracellular localization and nucleocytoplasmic trafficking of steroid receptors: an overview. Mol. Cell. Endocrinol. *246*, 147–156.
14. Larange, A., Takazawa, I., Kakugawa, K., Thiault, N., Ngoi, S., Olive, M.E., Iwaya, H., Seguin, L., Vicente-Suarez, I., Becart, S., et al. (2023). A regulatory circuit controlled by extranuclear and nuclear retinoic acid receptor α determines T cell activation and function. Immunity *56*, 2054–2069.e10.
15. Lavin, Y., Mortha, A., Rahman, A., and Merad, M. (2015). Regulation of macrophage development and function in peripheral tissues. Nat. Rev. Immunol. *15*, 731–744.
16. Wilkenfeld, S.R., Lin, C., and Frigo, D.E. (2018). Communication between genomic and non-genomic signaling events coordinate steroid hormone actions. Steroids *133*, 2–7.
17. Xu, Q., Jitkaew, S., Choksi, S., Kadigamuwa, C., Qu, J., Choe, M., Jang, J., Liu, C., and Liu, Z.G. (2017). The cytoplasmic nuclear receptor RARγ controls RIP1 initiated cell death when cIAP activity is inhibited. Nat. Commun. *8*, 425.
18. Zhu, F., Ma, J., Li, W., Liu, Q., Qin, X., Qian, Y., Wang, C., Zhang, Y., Li, Y., Jiang, D., et al. (2023). The orphan receptor Nur77 binds cytoplasmic LPS to activate the non-canonical NLRP3 inflammasome. Immunity *56*, 753–767.e8.
19. Barnes, P.J. (1998). Anti-inflammatory actions of glucocorticoids: molecular mechanisms. Clin. Sci. (Lond) *94*, 557–572.
20. Sun, Z., Unutmaz, D., Zou, Y.R., Sunshine, M.J., Pierani, A., Brenner-Morton, S., Mebius, R.E., and Littman, D.R. (2000). Requirement for RORgamma in thymocyte survival and lymphoid organ development. Science *288*, 2369–2373.
21. Winoto, A., and Littman, D.R. (2002). Nuclear hormone receptors in T lymphocytes. Cell *109*, S57–S66.
22. Kurebayashi, S., Ueda, E., Sakaue, M., Patel, D.D., Medvedev, A., Zhang, F., and Jetten, A.M. (2000). Retinoid-related orphan receptor γ (RORγ) is essential for lymphoid organogenesis and controls apoptosis during thymopoiesis. Proc. Natl. Acad. Sci. USA *97*, 10132–10137.
23. Eberl, G., and Littman, D.R. (2003). The role of the nuclear hormone receptor RORγt in the development of lymph nodes and Peyer's patches. Immunol. Rev. *195*, 81–90.
24. Korn, T., Bettelli, E., Oukka, M., and Kuchroo, V.K. (2009). IL-17 and Th17 cells. Annu. Rev. Immunol. *27*, 485–517.
25. Ramanan, D., Pratama, A., Zhu, Y., Venezia, O., Sassone-Corsi, M., Chowdhary, K., Galván-Peña, S., Sefik, E., Brown, C., Gélineau, A., et al. (2023). Regulatory T cells in the face of the intestinal microbiota. Nat. Rev. Immunol. *23*, 749–762.
26. Fassett, M.S., Jiang, W., D'Alise, A.M., Mathis, D., and Benoist, C. (2012). Nuclear receptor Nr4a1 modulates both regulatory T-cell (Treg) differentiation and clonal deletion. Proc. Natl. Acad. Sci. USA *109*, 3891–3896.
27. Sekiya, T., Kashiwagi, I., Yoshida, R., Fukaya, T., Morita, R., Kimura, A., Ichinose, H., Metzger, D., Chambon, P., and Yoshimura, A. (2013). Nr4a receptors are essential for thymic regulatory T cell development and immune homeostasis. Nat. Immunol. *14*, 230–237.
28. van de Pavert, S.A., Ferreira, M., Domingues, R.G., Ribeiro, H., Molenaar, R., Moreira-Santos, L., Almeida, F.F., Ibiza, S., Barbosa, I., Goverse, G., et al. (2014). Maternal retinoids control type 3 innate lymphoid cells and set the offspring immunity. Nature *508*, 123–127.
29. Okabe, Y., and Medzhitov, R. (2014). Tissue-specific signals control reversible program of localization and functional polarization of macrophages. Cell *157*, 832–844.
30. Casanova-Acebes, M., Menéndez-Gutiérrez, M.P., Porcuna, J., Álvarez-Errico, D., Lavin, Y., García, A., Kobayashi, S., Le Berichel, J., Núñez, V., Were, F., et al. (2020). RXRs control serous macrophage neonatal expansion and identity and contribute to ovarian cancer progression. Nat. Commun. *11*, 1655.
31. Geissmann, F., Revy, P., Brousse, N., Lepelletier, Y., Folli, C., Durandy, A., Chambon, P., and Dy, M. (2003). Retinoids regulate survival and antigen presentation by immature dendritic cells. J. Exp. Med. *198*, 623–634.
32. Hall, J.A., Grainger, J.R., Spencer, S.P., and Belkaid, Y. (2011). The role of retinoic acid in tolerance and immunity. Immunity *35*, 13–22.
33. Iwata, M., Hirakiyama, A., Eshima, Y., Kagechika, H., Kato, C., and Song, S.Y. (2004). Retinoic acid imprints gut-homing specificity on T cells. Immunity *21*, 527–538.

34. Mora, J.R., Iwata, M., Eksteen, B., Song, S.Y., Junt, T., Senman, B., Otipoby, K.L., Yokota, A., Takeuchi, H., Ricciardi-Castagnoli, P., et al. (2006). Generation of gut-homing IgA-secreting B cells by intestinal dendritic cells. Science *314*, 1157–1160.

35. Kim, M.H., Taparowsky, E.J., and Kim, C.H. (2015). Retinoic acid differentially regulates the migration of innate lymphoid cell subsets to the gut. Immunity *43*, 107–119.

36. Cabezas-Wallscheid, N., Buettner, F., Sommerkamp, P., Klimmeck, D., Ladel, L., Thalheimer, F.B., Pastor-Flores, D., Roma, L.P., Renders, S., Zeisberger, P., et al. (2017). Vitamin A-retinoic acid signaling regulates hematopoietic stem cell dormancy. Cell *169*, 807–823.e19.

37. Cipolletta, D., Feuerer, M., Li, A., Kamei, N., Lee, J., Shoelson, S.E., Benoist, C., and Mathis, D. (2012). PPAR-γ is a major driver of the accumulation and phenotype of adipose tissue Treg cells. Nature *486*, 549–553.

38. Michaels, A.J., Campbell, C., Bou-Puerto, R., and Rudensky, A.Y. (2021). Nuclear receptor LXRβ controls fitness and functionality of activated T cells. J. Exp. Med. *218*, e20201311.

39. Jones, B.G., Penkert, R.R., Surman, S.L., Sealy, R.E., and Hurwitz, J.L. (2020). Nuclear receptors, ligands and the mammalian B cell. Int. J. Mol. Sci. *21*, 4997.

40. Odagiu, L., May, J., Boulet, S., Baldwin, T.A., and Labrecque, N. (2020). Role of the orphan nuclear receptor NR4A family in T-cell biology. Front. Endocrinol. (Lausanne) *11*, 624122.

41. Kastner, P., Lawrence, H.J., Waltzinger, C., Ghyselinck, N.B., Chambon, P., and Chan, S. (2001). Positive and negative regulation of granulopoiesis by endogenous RARalpha. Blood *97*, 1314–1320.

42. Buechler, M.B., Kim, K.W., Onufer, E.J., Williams, J.W., Little, C.C., Dominguez, C.X., Li, Q., Sandoval, W., Cooper, J.E., Harris, C.A., et al. (2019). A stromal niche defined by expression of the transcription factor WT1 mediates programming and homeostasis of cavity-resident macrophages. Immunity *51*, 119–130.e5.

43. Larange, A., and Cheroutre, H. (2016). Retinoic acid and retinoic acid receptors as pleiotropic modulators of the immune system. Annu. Rev. Immunol. *34*, 369–394.

44. Baysoy, A., Seddu, K., Salloum, T., Dawson, C.A., Lee, J.J., Yang, L., Gal-Oz, S., Ner-Gaon, H., Tellier, J., Millan, A., et al. (2023). The interweaved signatures of common-gamma-chain cytokines across immunologic lineages. J. Exp. Med. *220*, e20222052.

45. Gautier, E.L., Shay, T., Miller, J., Greter, M., Jakubzick, C., Ivanov, S., Helft, J., Chow, A., Elpek, K.G., Gordonov, S., et al. (2012). Gene-expression profiles and transcriptional regulatory pathways that underlie the identity and diversity of mouse tissue macrophages. Nat. Immunol. *13*, 1118–1128.

46. Lavin, Y., Winter, D., Blecher-Gonen, R., David, E., Keren-Shaul, H., Merad, M., Jung, S., and Amit, I. (2014). Tissue-resident macrophage enhancer landscapes are shaped by the local microenvironment. Cell *159*, 1312–1326.

47. Gautier, E.L., Ivanov, S., Williams, J.W., Huang, S.C.C., Marcelin, G., Fairfax, K., Wang, P.L., Francis, J.S., Leone, P., Wilson, D.B., et al. (2014). Gata6 regulates aspartoacylase expression in resident peritoneal macrophages and controls their survival. J. Exp. Med. *211*, 1525–1531.

48. Rosas, M., Davies, L.C., Giles, P.J., Liao, C.T., Kharfan, B., Stone, T.C., O'Donnell, V.B., Fraser, D.J., Jones, S.A., and Taylor, P.R. (2014). The transcription factor Gata6 links tissue macrophage phenotype and proliferative renewal. Science *344*, 645–648.

49. Mass, E., Nimmerjahn, F., Kierdorf, K., and Schlitzer, A. (2023). Tissue-specific macrophages: how they develop and choreograph tissue biology. Nat. Rev. Immunol. *23*, 563–579.

50. Davies, L.C., Jenkins, S.J., Allen, J.E., and Taylor, P.R. (2013). Tissue-resident macrophages. Nat. Immunol. *14*, 986–995.

51. Gordon, S., Plüddemann, A., and Martinez Estrada, F. (2014). Macrophage heterogeneity in tissues: phenotypic diversity and functions. Immunol. Rev. *262*, 36–55.

52. Salm, L., Shim, R., Noskovicova, N., and Kubes, P. (2023). Gata6^{+} large peritoneal macrophages: an evolutionarily conserved sentinel and effector system for infection and injury. Trends Immunol. *44*, 129–145.

53. Honda, M., Kadohisa, M., Yoshii, D., Komohara, Y., and Hibi, T. (2021). Directly recruited GATA6 + peritoneal cavity macrophages contribute to the repair of intestinal serosal injury. Nat. Commun. *12*, 7294.

54. Zindel, J., Peiseler, M., Hossain, M., Deppermann, C., Lee, W.Y., Haenni, B., Zuber, B., Deniset, J.F., Surewaard, B.G.J., Candinas, D., et al. (2021). Primordial GATA6 macrophages function as extravascular platelets in sterile injury. Science *371*, eabe0595.

55. Qie, J., Liu, Y., Wang, Y., Zhang, F., Qin, Z., Tian, S., Liu, M., Li, K., Shi, W., Song, L., et al. (2022). Integrated proteomic and transcriptomic landscape of macrophages in mouse tissues. Nat. Commun. *13*, 7389.

56. Gonzalez, M.A., Girgis, N., Gundra, U.M., Tang, M.S., Vozhilla, N., and Loke, P. (2016). Vitamin A deficiency disrupts conversion of inflammatory monocyte derived M2 macrophages into a tissue resident macrophage phenotype. J. Immunol. *196*, 52.12.

57. Gundra, U.M., Girgis, N.M., Gonzalez, M.A., San Tang, M., Van Der Zande, H.J.P., Lin, J.D., Ouimet, M., Ma, L.J., Poles, J., Vozhilla, N., et al. (2017). Vitamin A mediates conversion of monocyte-derived macrophages into tissue-resident macrophages during alternative activation. Nat. Immunol. *18*, 642–653.

58. Philpott, J., Kazimierczyk, S., Korgaonkar, P., Bordt, E., Zois, J., Vasudevan, C., Meng, D., Bhatia, I., Lu, N., Jimena, B., et al. (2022). RXRalpha regulates the development of resident tissue macrophages. Immunohorizons *6*, 366–372.

59. Mimitou, E.P., Lareau, C.A., Chen, K.Y., Zorzetto-Fernandes, A.L., Hao, Y., Takeshima, Y., Luo, W., Huang, T.S., Yeung, B.Z., Papalexi, E., et al. (2021). Scalable, multimodal profiling of chromatin accessibility, gene expression and protein levels in single cells. Nat. Biotechnol. *39*, 1246–1258.

60. Finlay, C.M., Parkinson, J.E., Zhang, L., Chan, B.H.K., Ajendra, J., Chenery, A., Morrison, A., Kaymak, I., Houlder, E.L., Murtuza Baker, S., et al. (2023). T helper 2 cells control monocyte to tissue-resident macrophage differentiation during nematode infection of the pleural cavity. Immunity *56*, 1064–1081.e10.

61. Han, J., Gallerand, A., Erlich, E.C., Helmink, B.A., Mair, I., Li, X., Eckhouse, S.R., Dimou, F.M., Shakhsheer, B.A., Phelps, H.M., et al. (2024). Human serous cavity macrophages and dendritic cells possess counterparts in the mouse with a distinct distribution between species. Nat. Immunol. *25*, 155–165.

62. Bain, C.C., Hawley, C.A., Garner, H., Scott, C.L., Schridde, A., Steers, N.J., Mack, M., Joshi, A., Guilliams, M., Mowat, A.M.I., et al. (2016). Long-lived self-renewing bone marrow-derived macrophages displace embryo-derived cells to inhabit adult serous cavities. Nat. Commun. *7*, ncomms11852.

63. Goudot, C., Coillard, A., Villani, A.C., Gueguen, P., Cros, A., Sarkizova, S., Tang-Huau, T.L., Bohec, M., Baulande, S., Hacohen, N., et al. (2017). Aryl hydrocarbon receptor Controls monocyte Differentiation into dendritic Cells versus Macrophages. Immunity *47*, 582–596.e6.

64. Bain, C.C., Louwe, P.A., Steers, N.J., Bravo-Blas, A., Hegarty, L.M., Pridans, C., Milling, S.W.F., MacDonald, A.S., Rückerl, D., and Jenkins, S.J. (2022). CD11c identifies microbiota and EGR2-dependent MHCII^{+} serous cavity macrophages with sexually dimorphic fate in mice. Eur. J. Immunol. *52*, 1243–1257.

65. Prat, M., Coulson, K., Blot, C., Jacquemin, G., Romano, M., Renoud, M.L., AlaEddine, M., Le Naour, A., Authier, H., Rahabi, M.C., et al. (2023). PPARγ activation modulates the balance of peritoneal macrophage populations to suppress ovarian tumor growth and tumor-induced immunosuppression. J. Immunother. Cancer *11*, e007031.

66. Gustafsson, C., De Paepe, A., Schmidl, C., and Månsson, R. (2019). High-throughput ChIPmentation: freely scalable, single day ChIPseq data generation from very low cell-numbers. BMC Genomics *20*, 59.

67. Holmes, W.F., Dawson, M.I., Soprano, R.D., and Soprano, K.J. (2000). Induction of apoptosis in ovarian carcinoma cells by AHPN/CD437 is mediated by retinoic acid receptors. J. Cell. Physiol. *185*, 61–67.

68. Klaholz, B.P., Renaud, J.P., Mitschler, A., Zusi, C., Chambon, P., Gronemeyer, H., and Moras, D. (1998). Conformational adaptation of agonists to the human nuclear receptor RARγ. Nat. Struct. Biol. *5*, 199–202.

69. Zhang, N., Czepielewski, R.S., Jarjour, N.N., Erlich, E.C., Esaulova, E., Saunders, B.T., Grover, S.P., Cleuren, A.C., Broze, G.J., Edelson, B.T., et al. (2019). Expression of factor V by resident macrophages boosts host defense in the peritoneal cavity. J. Exp. Med. *216*, 1291–1300.

70. Vega-Pérez, A., Villarrubia, L.H., Godio, C., Gutiérrez-González, A., Feo-Lucas, L., Ferriz, M., Martínez-Puente, N., Alcaín, J., Mora, A., Sabio, G., et al. (2021). Resident macrophage-dependent immune cell scaffolds drive anti-bacterial defense in the peritoneal cavity. Immunity *54*, 2578–2594.e5.

71. Zen, K., Guo, Y.L., Li, L.M., Bian, Z., Zhang, C.Y., and Liu, Y. (2011). Cleavage of the CD11b extracellular domain by the leukocyte serprocidins is critical for neutrophil detachment during chemotaxis. Blood *117*, 4885–4894.

72. Aglietti, R.A., Estevez, A., Gupta, A., Ramirez, M.G., Liu, P.S., Kayagaki, N., Ciferri, C., Dixit, V.M., and Dueber, E.C. (2016). GsdmD p30 elicited by caspase-11 during pyroptosis forms pores in membranes. Proc. Natl. Acad. Sci. USA *113*, 7858–7863.

73. Sagulenko, V., Thygesen, S.J., Sester, D.P., Idris, A., Cridland, J.A., Vajjhala, P.R., Roberts, T.L., Schroder, K., Vince, J.E., Hill, J.M., et al. (2013). AIM2 and NLRP3 inflammasomes activate both apoptotic and pyroptotic death pathways via ASC. Cell Death Differ. *20*, 1149–1160.

74. Bertheloot, D., Latz, E., and Franklin, B.S. (2021). Necroptosis, pyroptosis and apoptosis: an intricate game of cell death. Cell. Mol. Immunol. *18*, 1106–1121.

75. Pandeya, A., and Kanneganti, T.D. (2024). Therapeutic potential of panoptosis: innate sensors, inflammasomes, and RIPKs in PANoptosomes. Trends Mol. Med. *30*, 74–88.

76. Weng, D., Marty-Roix, R., Ganesan, S., Proulx, M.K., Vladimer, G.I., Kaiser, W.J., Mocarski, E.S., Pouliot, K., Chan, F.K.M., Kelliher, M.A., et al. (2014). Caspase-8 and RIP kinases regulate bacteria-induced innate immune responses and cell death. Proc. Natl. Acad. Sci. USA *111*, 7391–7396.

77. Rathinam, V.A.K., and Fitzgerald, K.A. (2016). Inflammasome complexes: emerging mechanisms and effector functions. Cell *165*, 792–800.

78. Suzuki, S., Franchi, L., He, Y., Muñoz-Planillo, R., Mimuro, H., Suzuki, T., Sasakawa, C., and Núñez, G. (2014). Shigella type III secretion protein MxiI is recognized by Naip2 to induce Nlrc4 inflammasome activation independently of Pkcdelta. PLoS Pathog. *10*, e1003926.

79. Renaud, J.P., Rochel, N., Ruff, M., Vivat, V., Chambon, P., Gronemeyer, H., and Moras, D. (1995). Crystal structure of the RAR-γ ligand-binding domain bound to all-trans retinoic acid. Nature *378*, 681–689.

80. Hughes, N.E., Bleisch, T.J., Jones, S.A., Richardson, T.I., Doti, R.A., Wang, Y., Stout, S.L., Durst, G.L., Chambers, M.G., Oskins, J.L., et al. (2016). Identification of potent and selective retinoic acid receptor gamma (RARgamma) antagonists for the treatment of osteoarthritis pain using structure based drug design. Bioorg. Med. Chem. Lett. *26*, 3274–3277.

81. Zhang, P., Liu, Y., Hu, L., Huang, K., Hong, M., Wang, Y., Fan, X., Ulevitch, R.J., and Han, J. (2021). NLRC4 inflammasome-dependent cell death occurs by a complementary series of three death pathways and determines lethality in mice. Sci. Adv. *7*, eabi9471.

82. Chen, C., Zhou, Y., Ning, X., Li, S., Xue, D., Wei, C., Zhu, Z., Sheng, L., Lu, B., Li, Y., et al. (2022). Directly targeting ASC by lonidamine alleviates inflammasome-driven diseases. J. Neuroinflammation *19*, 315.

83. Schroder, K., and Tschopp, J. (2010). The inflammasomes. Cell *140*, 821–832.

84. Van Opdenbosch, N., Gurung, P., Vande Walle, L., Fossoul, A., Kanneganti, T.D., and Lamkanfi, M. (2014). Activation of the NLRP1b inflammasome independently of ASC-mediated caspase-1 autoproteolysis and speck formation. Nat. Commun. *5*, 3209.

85. Broz, P., von Moltke, J., Jones, J.W., Vance, R.E., and Monack, D.M. (2010). Differential requirement for caspase-1 autoproteolysis in pathogen-induced cell death and cytokine processing. Cell Host Microbe *8*, 471–483.

86. Lin, S.J., Yang, D.R., Yang, G., Lin, C.Y., Chang, H.C., Li, G., and Chang, C. (2017). TR2 and TR4 orphan nuclear receptors: an overview. Curr. Top. Dev. Biol. *125*, 357–373.

87. Schneider, C., Nobs, S.P., Kurrer, M., Rehrauer, H., Thiele, C., and Kopf, M. (2014). Induction of the nuclear receptor PPAR-γ by the cytokine GM-CSF is critical for the differentiation of fetal monocytes into alveolar macrophages. Nat. Immunol. *15*, 1026–1037.

88. Guilliams, M., De Kleer, I., Henri, S., Post, S., Vanhoutte, L., De Prijck, S., Deswarte, K., Malissen, B., Hammad, H., and Lambrecht, B.N. (2013). Alveolar macrophages develop from fetal monocytes that differentiate into long-lived cells in the first week of life via GM-CSF. J. Exp. Med. *210*, 1977–1992.

89. A-Gonzalez, N., Guillen, J.A., Gallardo, G., Diaz, M., de la Rosa, J.V., Hernandez, I.H., Casanova-Acebes, M., Lopez, F., Tabraue, C., Beceiro, S., et al. (2013). The nuclear receptor LXRα controls the functional specialization of splenic macrophages. Nat. Immunol. *14*, 831–839.

90. Schmidt, S., Rainer, J., Ploner, C., Presul, E., Riml, S., and Kofler, R. (2004). Glucocorticoid-induced apoptosis and glucocorticoid resistance: molecular mechanisms and clinical relevance. Cell Death Differ. *11*, S45–S55.

91. Noy, N. (2010). Between death and survival: retinoic acid in regulation of apoptosis. Annu. Rev. Nutr. *30*, 201–217.

92. Yoshida, H., Lareau, C.A., Ramirez, R.N., Rose, S.A., Maier, B., Wroblewska, A., Desland, F., Chudnovskiy, A., Mortha, A., Dominguez, C., et al. (2019). The cis-regulatory atlas of the mouse immune system. Cell *176*, 897–912.e20.

93. Wang, W., Wu, S., Cen, Z., Zhang, Y., Chen, Y., Huang, Y., Cillo, A.R., Prokopec, J.S., Quarato, G., Vignali, D.A.A., et al. (2022). Mobilizing phospholipids on tumor plasma membrane implicates phosphatidylserine externalization blockade for cancer immunotherapy. Cell Rep. *41*, 111582.

94. Tomura, M., Yoshida, N., Tanaka, J., Karasawa, S., Miwa, Y., Miyawaki, A., and Kanagawa, O. (2008). Monitoring cellular movement in vivo with photoconvertible fluorescence protein "Kaede" transgenic mice. Proc. Natl. Acad. Sci. USA *105*, 10871–10876.

95. Morton, A.M., Sefik, E., Upadhyay, R., Weissleder, R., Benoist, C., and Mathis, D. (2014). Endoscopic photoconversion reveals unexpectedly broad leukocyte trafficking to and from the gut. Proc. Natl. Acad. Sci. USA *111*, 6696–6701.

96. Liston, A., Nutsch, K.M., Farr, A.G., Lund, J.M., Rasmussen, J.P., Koni, P.A., and Rudensky, A.Y. (2008). Differentiation of regulatory $Foxp3^+$ T cells in the thymic cortex. Proc. Natl. Acad. Sci. USA *105*, 11903–11908.

97. Hise, A.G., Tomalka, J., Ganesan, S., Patel, K., Hall, B.A., Brown, G.D., and Fitzgerald, K.A. (2009). An essential role for the NLRP3 inflammasome in host defense against the human fungal pathogen Candida albicans. Cell Host Microbe *5*, 487–497.

98. Heinz, S., Benner, C., Spann, N., Bertolino, E., Lin, Y.C., Laslo, P., Cheng, J.X., Murre, C., Singh, H., and Glass, C.K. (2010). Simple combinations of lineage-determining transcription factors prime cis-regulatory elements required for macrophage and B cell identities. Mol. Cell *38*, 576–589.

99. van der Maaten, L., and Hinton, G. (2008). Visualizing high-dimensional data using t-SNE. J. Mach. Learn. Res. *9*, 2579–2605.

100. Robinson, J.T., Thorvaldsdóttir, H., Winckler, W., Guttman, M., Lander, E.S., Getz, G., and Mesirov, J.P. (2011). Integrative genomics viewer. Nat. Biotechnol. *29*, 24–26.

101. Quinlan, A.R., and Hall, I.M. (2010). BEDTools: a flexible suite of utilities for comparing genomic features. Bioinformatics *26*, 841–842.

102. Langmead, B., and Salzberg, S.L. (2012). Fast gapped-read alignment with Bowtie 2. Nat. Methods *9*, 357–359.

103. Schep, A.N., Wu, B., Buenrostro, J.D., and Greenleaf, W.J. (2017). chromVAR: inferring transcription-factor-associated accessibility from single-cell epigenomic data. Nat. Methods *14*, 975–978.

104. Hao, Y., Hao, S., Andersen-Nissen, E., Mauck, W.M., III, Zheng, S., Butler, A., Lee, M.J., Wilk, A.J., Darby, C., Zager, M., et al. (2021). Integrated analysis of multimodal single-cell data. Cell *184*, 3573–3587.e29.

105. Zhang, Y., Liu, T., Meyer, C.A., Eeckhoute, J., Johnson, D.S., Bernstein, B.E., Nusbaum, C., Myers, R.M., Brown, M., Li, W., et al. (2008). Model-based analysis of ChIP-Seq (MACS). Genome Biol. *9*, R137.

106. Ramírez, F., Ryan, D.P., Grüning, B., Bhardwaj, V., Kilpert, F., Richter, A.S., Heyne, S., Dündar, F., and Manke, T. (2016). deepTools2: a next generation web server for deep-sequencing data analysis. Nucleic Acids Res. *44*, W160–W165.

107. Li, H., Handsaker, B., Wysoker, A., Fennell, T., Ruan, J., Homer, N., Marth, G., Abecasis, G., and Durbin, R.; 1000 Genome Project Data Processing Subgroup (2009). The Sequence Alignment/Map format and SAMtools. Bioinformatics *25*, 2078–2079.

108. Dobin, A., Davis, C.A., Schlesinger, F., Drenkow, J., Zaleski, C., Jha, S., Batut, P., Chaisson, M., and Gingeras, T.R. (2013). STAR: ultrafast universal RNA-seq aligner. Bioinformatics *29*, 15–21.

109. Liao, Y., Smyth, G.K., and Shi, W. (2014). featureCounts: an efficient general purpose program for assigning sequence reads to genomic features. Bioinformatics *30*, 923–930.

110. Love, M.I., Huber, W., and Anders, S. (2014). Moderated estimation of fold change and dispersion for RNA-seq data with DESeq2. Genome Biol. *15*, 550.

111. Wang, L., Nie, J., Sicotte, H., Li, Y., Eckel-Passow, J.E., Dasari, S., Vedell, P.T., Barman, P., Wang, L., Weinshiboum, R., et al. (2016). Measure transcript integrity using RNA-seq data. BMC Bioinformatics *17*, 58.

112. Clement, K., Rees, H., Canver, M.C., Gehrke, J.M., Farouni, R., Hsu, J.Y., Cole, M.A., Liu, D.R., Joung, J.K., Bauer, D.E., et al. (2019). CRISPResso2 provides accurate and rapid genome editing sequence analysis. Nat. Biotechnol. *37*, 224–226.

113. Platt, R.J., Chen, S., Zhou, Y., Yim, M.J., Swiech, L., Kempton, H.R., Dahlman, J.E., Parnas, O., Eisenhaure, T.M., Jovanovic, M., et al. (2014). CRISPR-Cas9 knockin mice for genome editing and cancer modeling. Cell *159*, 440–455.

114. Kovarova, M., Hesker, P.R., Jania, L., Nguyen, M., Snouwaert, J.N., Xiang, Z., Lommatzsch, S.E., Huang, M.T., Ting, J.P.Y., and Koller, B.H. (2012). NLRP1-dependent pyroptosis leads to acute lung injury and morbidity in mice. J. Immunol. *189*, 2006–2016.

115. Kuida, K., Lippke, J.A., Ku, G., Harding, M.W., Livingston, D.J., Su, M.S., and Flavell, R.A. (1995). Altered cytokine export and apoptosis in mice deficient in interleukin-1 β converting enzyme. Science *267*, 2000–2003.

116. Shi, J., Zhao, Y., Wang, K., Shi, X., Wang, Y., Huang, H., Zhuang, Y., Cai, T., Wang, F., and Shao, F. (2015). Cleavage of GSDMD by inflammatory caspases determines pyroptotic cell death. Nature *526*, 660–665.

117. Doench, J.G., Fusi, N., Sullender, M., Hegde, M., Vaimberg, E.W., Donovan, K.F., Smith, I., Tothova, Z., Wilen, C., Orchard, R., et al. (2016). Optimized sgRNA design to maximize activity and minimize off-target effects of CRISPR-Cas9. Nat. Biotechnol. *34*, 184–191.

118. Sanson, K.R., Hanna, R.E., Hegde, M., Donovan, K.F., Strand, C., Sullender, M.E., Vaimberg, E.W., Goodale, A., Root, D.E., Piccioni, F., et al. (2018). Optimized libraries for CRISPR-Cas9 genetic screens with multiple modalities. Nat. Commun. *9*, 5416.

119. Sanjana, N.E., Shalem, O., and Zhang, F. (2014). Improved vectors and genome-wide libraries for CRISPR screening. Nat. Methods *11*, 783–784.

120. Wang, T., Yu, H., Hughes, N.W., Liu, B., Kendirli, A., Klein, K., Chen, W.W., Lander, E.S., and Sabatini, D.M. (2017). Gene essentiality profiling reveals gene networks and synthetic lethal interactions with oncogenic Ras. Cell *168*, 890–903.e15.

121. Picelli, S., Björklund, Å.K., Faridani, O.R., Sagasser, S., Winberg, G., and Sandberg, R. (2013). Smart-seq2 for sensitive full-length transcriptome profiling in single cells. Nat. Methods *10*, 1096–1098.

122. Picelli, S., Faridani, O.R., Björklund, A.K., Winberg, G., Sagasser, S., and Sandberg, R. (2014). Full-length RNA-seq from single cells using Smart-seq2. Nat. Protoc. *9*, 171–181.

123. Stoeckius, M., Zheng, S., Houck-Loomis, B., Hao, S., Yeung, B.Z., Mauck, W.M., III, Smibert, P., and Satija, R. (2018). Cell hashing with barcoded antibodies enables multiplexing and doublet detection for single cell genomics. Genome Biol. *19*, 224.

124. Schmidl, C., Rendeiro, A.F., Sheffield, N.C., and Bock, C. (2015). ChIPmentation: fast, robust, low-input ChIP-seq for histones and transcription factors. Nat. Methods *12*, 963–965.

125. Buenrostro, J.D., Wu, B., Litzenburger, U.M., Ruff, D., Gonzales, M.L., Snyder, M.P., Chang, H.Y., and Greenleaf, W.J. (2015). Single-cell chromatin accessibility reveals principles of regulatory variation. Nature *523*, 486–490.

126. Nordin, A., Zambanini, G., Pagella, P., and Cantù, C. (2023). The CUT&RUN suspect list of problematic regions of the genome. Genome Biol. *24*, 185.

127. Ramírez, F., Dündar, F., Diehl, S., Grüning, B.A., and Manke, T. (2014). deepTools: a flexible platform for exploring deep-sequencing data. Nucleic Acids Res. *42*, W187–W191.

128. Sandstrom, A., Mitchell, P.S., Goers, L., Mu, E.W., Lesser, C.F., and Vance, R.E. (2019). Functional degradation: A mechanism of NLRP1 inflammasome activation by diverse pathogen enzymes. Science *364*, eaau1330.

129. Guo, H., and Ting, J.P.Y. (2020). Inflammasome assays in vitro and in mouse models. Curr. Protoc. Immunol. *131*, e107.

Please cite this article in press as: Wang et al., A pan-family screen of nuclear receptors in immunocytes reveals ligand-dependent inflammasome control, Immunity (2024), https://doi.org/10.1016/j.immuni.2024.10.010

STAR★METHODS

KEY RESOURCES TABLE

REAGENT or RESOURCE	SOURCE	IDENTIFIER
Antibodies		
anti-mouse CD103 (clone W19396D), PE	Biolegend	Cat# 110903; RRID:AB_2927994
anti-mouse CD115 (CSF-1R) (clone AFS98), Alexa Fluor® 488	Biolegend	Cat# 135511; RRID:AB_11218605
anti-mouse CD117 (c-Kit) (clone 2B8), PE/Cyanine7	Biolegend	Cat# 105814; RRID:AB_313223
anti-mouse CD11c (clone N418), APC, Alexa Fluor® 700, PE, PE/Cyanine7, Biotin	Biolegend	Cat# 117310; RRID:AB_313779; Cat# 117320; RRID:AB_528736; Cat# 117308; RRID:AB_313777; Cat# 117318; RRID:AB_493568; Cat# 117304; RRID:AB_313773
anti-mouse CD138 (clone 281-2), Brilliant Violet 711™	Biolegend	Cat# 142519; RRID:AB_2562571
anti-mouse CD169 (Siglec-1) (clone 3D6.112), PE/Cyanine7	Biolegend	Cat# 142412; RRID:AB_2563911
anti-mouse CD19 (clone 6D5), Brilliant Violet 605™, Alexa Fluor® 700, PE/Cyanine7, PE, Biotin	Biolegend	Cat# 115540; RRID:AB_2563067; Cat# 115528; RRID:AB_493735; Cat# 115520; RRID:AB_313655; Cat# 115508; RRID:AB_313643; Cat# 115504; RRID:AB_313639
anti-mouse CD209a (DC-SIGN) (clone MMD3), APC	Biolegend	Cat# 833005; RRID:AB_2927969
anti-mouse CD206 (MMR) (clone C068C2), APC	Biolegend	Cat# 141707; RRID:AB_10896057
anti-mouse CD21/CD35 (clone 7E9), PerCP/Cyanine5.5	Biolegend	Cat# 123415; RRID:AB_1595595
anti-mouse CD23 (clone B3B4), Alexa Fluor® 647	Biolegend	Cat# 101612; RRID:AB_2103038
anti-mouse CD301b (MGL2) (Clone URA-1), PE/Cyanine7	Biolegend	Cat# 146808; RRID:AB_2563390
anti-mouse CD317 (pDCA1) (clone 927), Brilliant Ultra Violet™ 737	BD Biosciences	Cat# 749272; RRID:AB_2873649
anti-mouse CD38 (clone 90), Brilliant Violet 421™	Biolegend	Cat# 102732; RRID:AB_2734153
anti-mouse CD4 (clone RM4-5), Brilliant Violet 711™, Alexa Fluor® 700, PE, Biotin	Biolegend	Cat# 100557; RRID:AB_2562607; Cat# 100536; RRID:AB_493701; Cat# 100512; RRID:AB_312715; Cat# 100507; RRID:AB_312710
anti-mouse CD45.2 (clone 104), APC/Cyanine7, APC, Alexa Fluor® 700	Biolegend	Cat# 109824; RRID:AB_830789; Cat# 109814; RRID:AB_389211; Cat# 109822; RRID:AB_493731
anti-mouse CD45.1 (clone A20), Alexa Fluor® 700	Biolegend	Cat# 110723; RRID:AB_493732
anti-mouse CD62L (clone MEL-14), Brilliant Violet 785™	Biolegend	Cat# 104440; RRID:AB_2629685
anti-mouse CD64 (FcγRI) (clone X54-5/7.1), APC	Biolegend	Cat# 139306; RRID:AB_11219391
anti-mouse CD68 (clone FA-11), PE	Biolegend	Cat# 137013; RRID:AB_10613469
anti-mouse CD8a (clone 53-6.7), Alexa Fluor® 700, PE, Biotin	Biolegend	Cat# 100730; RRID:AB_493703; Cat# 100708; RRID:AB_312747; Cat# 100704; RRID:AB_312743
anti-mouse CD93 (clone AA4.1), PE/Cyanine7	Biolegend	Cat# 136506; RRID:AB_2044012
anti-mouse CD95 (Fas) (clone Jo2), Brilliant Ultra Violet™737	BD Biosciences	Cat# 741763; RRID:AB_2871122
anti-mouse F4/80 (clone BM8), Brilliant Violet 785™	Biolegend	Cat# 123141; RRID:AB_2563667
anti-mouse I-A/I-E (MHC-II) (M5/114.15.2), Brilliant Violet 605™	Biolegend	Cat# 107639; RRID:AB_2565894
anti-mouse IgD (clone 11-26c.2a), Brilliant Violet 510™, PE	Biolegend	Cat# 405723; RRID:AB_2562742; Cat# 405705; RRID:AB_315027
anti-mouse IgM (clone RMM-1), Brilliant Violet 605™	Biolegend	Cat# 406523; RRID:AB_2563358
anti-mouse Ly-6A/E (Sca-1) (clone D7), APC	Biolegend	Cat# 108112; RRID:AB_313349

(*Continued on next page*)

Please cite this article in press as: Wang et al., A pan-family screen of nuclear receptors in immunocytes reveals ligand-dependent inflammasome control, Immunity (2024), https://doi.org/10.1016/j.immuni.2024.10.010

Continued

REAGENT or RESOURCE	SOURCE	IDENTIFIER
anti-mouse Ly-6C (clone HK1.4), Brilliant Violet 711™, Alexa Fluor 700®, PE, Biotin	Biolegend	Cat# 128037; RRID:AB_2562630; Cat# 128024; RRID:AB_10643270; Cat# 128008; RRID:AB_1186132; Cat# 128004; RRID:AB_1236553
anti-mouse Ly-6G (clone 1A8), Brilliant Violet 421™, Alexa Fluor® 700, PE, Biotin	Biolegend	Cat# 127628; RRID:AB_2562567; Cat# 127622; RRID:AB_10643269; Cat# 127608; RRID:AB_1186099; Cat# 127604; RRID:AB_1186108
anti-mouse Ly-6G/Ly-6C (Gr-1)(clone RB6-8C5), PE, Biotin	Biolegend	Cat# 108407; RRID:AB_313372; Cat# 108403; RRID:AB_313368
anti-mouse NK1.1 (clone PK136), PE, Biotin	Biolegend	Cat# 108708; RRID:AB_313395; Cat# 108704; RRID:AB_313391
anti-mouse Siglec-F (clone E50-2440), APC-R700	BD Biosciences	Cat# 565183; RRID:AB_2739097
anti-mouse TCRβ Chain (clone H57-597), Brilliant Ultra Violet™737	BD Biosciences	Cat# 612821; RRID:AB_2870145
anti-mouse TCRγ/δ (clone GL3), Brilliant Violet 605™	Biolegend	Cat# 118129; RRID:AB_2563356
anti-mouse TER-119 (clone TER-119), PE, Biotin	Biolegend	Cat# 116208; RRID:AB_313709; Cat# 116204; RRID:AB_313705
anti-mouse/human CD11b (clone M1/70), PerCP/Cyanine5.5, FITC, Brilliant Violet 605™, Biotin	Biolegend	Cat# 101228; RRID:AB_893232; Cat# 101206; RRID:AB_312789; Cat# 101257; RRID:AB_2565431; Cat# 101204; RRID:AB_312787
anti-mouse/human CD44 (clone IM7), Brilliant Violet 510™	Biolegend	Cat# 103044; RRID:AB_2650923
anti-rat CD90/mouse CD90.1 (Thy-1.1) (clone OX-7), APC	Biolegend	Cat# 202526; RRID:AB_1595470
Annexin V PE	Biolegend	Cat# 640908; RRID:AB_2561298
TotalSeq-A anti-mouse hashtags antibody (clone M1/42; 30-F11)	Biolegend	Cat#155801; RRID:AB_2750032; Cat#155803; RRID:AB_2750033; Cat#155805; RRID:AB_2750034; Cat#155807; RRID:AB_2750035; Cat#155841; RRID:AB_2814072; Cat#155815; RRID:AB_2750040; Cat#155821; RRID:AB_2750136; Cat#155823; RRID:AB_2750137
anti-GATA-6 (clone D61E4), PE	Cell signal technology	Cat# 26452; RRID:AB_2798924
anti-RXRα (D6H10) rabbit mAb	Cell signal technology	Cat# 3085; RRID:AB_11140620
Rabbit IgG	Cell signal technology	Cat# 2729; RRID:AB_1031062
anti-RARγ rabbit polyclonal antibody	Proteintech	Cat# 11424-1-AP; RRID:AB_2175394
anti-RARγ mouse mAb	Santacruz	Cat# sc-7387; RRID:AB_2253411
anti-Caspase-1 (p20) mouse mAb (Casper-1)	AdipoGen	Cat# AG-20B-0042-C100
anti-Caspase-3 antibody	Cell signal technology	Cat# 9662; RRID:AB_331439
anti-cleaved Caspase-3 (Asp175) antibody	Cell signal technology	Cat# 9661; RRID:AB_2341188
anti-Caspase-7 antibody (10-1-62) antibody	Santacruz	Cat# sc-56063; RRID:AB_781833
anti-Caspase-8 antibody (1.1.40) antibody	Santacruz	Cat# sc-81656; RRID:AB_1120012
anti-PARP antibody	Cell signal technology	Cat# 9542; RRID:AB_2160739
anti-GAPDH antibody	Abcam	Cat# ab9484; RRID:AB_307274
anti-GSDMD antibody [EPR19828]	Abcam	Cat# ab209845; RRID:AB_2783550
anti-GSDMDC1 (H-11) antibody	Santacruz	Cat# sc-393581; RRID:AB_2819179
anti-GATA-6 (F-3) antibody	Santacruz	Cat# sc-518050
anti-ASC/TMS1 (D2W8U) rabbit mAb	Cell signal technology	Cat# 67824; RRID:AB_2799736
anti-NLRP3/NALP3, mAb (Cryo-2)	AdipoGen	Cat# AG-20B-0014-C100

(*Continued on next page*)

Please cite this article in press as: Wang et al., A pan-family screen of nuclear receptors in immunocytes reveals ligand-dependent inflammasome control, Immunity (2024), https://doi.org/10.1016/j.immuni.2024.10.010

Continued

REAGENT or RESOURCE	SOURCE	IDENTIFIER
HRP-Goat Anti-Rabbit IgG (H+L)	Jackson Immunoresearch	Cat# 111-035-144; RRID:AB_2307391
HRP-Donkey Anti-Mouse IgG (H+L)	Jackson Immunoresearch	Cat# 715-035-150; RRID:AB_2340770
HRP-Goat Anti-Mouse IgG, Light chain specific	Jackson Immunoresearch	Cat#115-035-174; RRID:AB_2338512
Goat anti-rabbit IgG H&L (Alexa Fluor® 488)	Abcam	Cat# ab150077; RRID:AB_2630356
Bacterial and virus strains		
Shigella flexneri 2457T	Dr. Lesser (Harvard University)	N/A
Chemicals, peptides, and recombinant proteins		
Zombie UV™ Fixable Viability Kit	Biolegend	Cat# 423107
Propidium Iodide	Sigma-Aldrich	Cat# 81845
DAPI (4',6-Diamidino-2-Phenylindole)	Biolegend	Cat# 422801
Goat Serum, New Zealand origin	Invitrogen	Cat# 16210064
Collagenase, Type IV	Gibco	Cat# 17104019
Collagenase, Type II	Gibco	Cat# 1701015
Collagenase, Type II	Sigma-Aldrich	Cat# C6885
Dispase	Gibco	Cat# 17105041
Deoxyribonuclease I, from bovine pancreas	Sigma-Aldrich	Cat# D4527
Digitonin	Sigma-Aldrich	Cat# D141
TCL RNA lysis buffer	Qiagen	Cat# 1031576
Bovine Serum Albumin(BSA), Fraction V	Research products international	Cat# A30075
DMEM, high glucose, no glutamine, no phenol red	Gibco	Cat# 31053028
RPMI 1640 Medium	Gibco	Cat# 11875119
DMEM F12	Gibco	Cat# 10565018
Opti-MEM™ I Reduced-Serum Medium	Gibco	Cat# 31985-070
StemPro™-34 SFM	Gibco	Cat# 10639011
Dynabeads™ Biotin Binder	Invitrogen	Cat# 11047
Anti-FLAG® M2 Magnetic Beads	Sigma-Aldrich	Cat# M8823
2-Mercaptoethanol	Sigma-Aldrich	Cat# M7522
Percoll	GE Healthcare	Cat# GE17-0891-01
16% formaldehyde	Thermo Fisher Scientific	Cat# 28906
T4 Polynucleotide Kinase	New England Biolabs	Cat# M0201S
BsmBI-v2	New England Biolabs	Cat# R0739L
DNA Ligation Kit, Mighty Mix	Takara	Cat# 6023
One Shot™ Stbl3™ Chemically Competent E. coli	Life Technologies	Cat# C7373-03
TransIT®-293 Transfection Reagent	Mirus	Cat# MIR 2705
Lipofectamine™ 3000 Transfection Reagent	Invitrogen	Cat#L3000001
PEG-it Virus Precipitation Solution	SBI	Cat# LV825A-1
Retronectin	TaKaRa	Cat# T100A
Recombinant Murine TPO	Peprotech	Cat# 315-14
Recombinant Murine SCF	Peprotech	Cat# 250-03
Recombinant Murine IL-7	Peprotech	Cat# 217-17
Recombinant Murine Flt3-Ligand	Peprotech	Cat# 250-31L
Recombinant protective antigen	Dr. Vance (UC Berkeley)	N/A
Recombinant lethal factor	Dr. Vance (UC Berkeley)	N/A
Dynabeads™ Protein A for Immunoprecipitation	Invitrogen	Cat# 10001D
AMPure XP SPRI Reagent	BeckmanCoulter	Cat# A63881
Ampicillin sodium salt	Sigma-Aldrich	Cat# A0166
LB Agar, Miller	BD	Cat# 244520
LB Broth, Miller	BD	Cat# 244620
Lipopolysaccharides from *Escherichia coli* O55:B5	Sigma-Aldrich	Cat# L2880

(*Continued on next page*)

Please cite this article in press as: Wang et al., A pan-family screen of nuclear receptors in immunocytes reveals ligand-dependent inflammasome control, Immunity (2024), https://doi.org/10.1016/j.immuni.2024.10.010

Continued

REAGENT or RESOURCE	SOURCE	IDENTIFIER
Adenosine 5'-triphosphate disodium salt	InvivoGen	Cat# tlrl-atpl
Nigericin sodium salt	InvivoGen	Cat# tlrl-nig
Poly(dA:dT)	InvivoGen	Cat# tlrl-patn
LY2955303 (RARγ antagonist)	Tocris	Cat# 5984
MM11253 (RARγ antagonist)	Tocris	Cat# 3822
BMS195614 (RARα antagonist)	Tocris	Cat# 3660
PA452 (RXR antagonist)	Tocris	Cat# 5086
BMS961(RARγ agonist)	Tocris	Cat# 3410
CD437 (RARγ agonist)	Tocris	Cat# 1549
CD2314(RARβ agonist)	Tocris	Cat# 3824
BMS753 (RARα agonist)	Tocris	Cat# 3505
CD3254 (RXRα agonist)	Tocris	Cat# 3302
cOmplete™, EDTA-free Protease Inhibitor Cocktail	Roche	Cat#11873580001
Z-DEVD-FMK (Caspase-3 inhibitor)	MedChemExpress	Cat# 210344-95-9
VX765 (Caspase-1 inhibitor)	Tocris	Cat# 7143
Q-VD-OPh (pan-caspase inhibitor)	MedChemExpress	Cat# HY-12305
Lonidamine (ASC inhibitor)	Tocris	Cat# 1646
Necrostatin-1(RIPK1 inhibitor)	Tocris	Cat# 2324
Critical commercial assays		
Illumina Tagment DNA Enzyme and Buffer Kit	Illumina	Cat# 20034197
QIAprep Spin Miniprep Kit	QIAGEN	Cat# 27106
NucleoSpin® Gel and PCR Clean-Up	TaKaRa	Cat# 740609.50
PicoPure™ DNA Extraction Kit	Thermo Fisher	Cat# KIT0103
Lumit™ Mouse IL-1β Immunoassay	Promega	Cat# W7010
LDH-Glo™ Cytotoxicity Assay	Promega	Cat# J2380
MinElute Reaction Cleanup Kit	QIAGEN	Cat# 28204
NEBNext High-Fidelity 2X PCR Master Mix	NEB	Cat# M0541
Chromium Single Cell Gene Expression 3' v3	10X Genomics	Cat# 1000269
Deposited data		
Bulk RNA-seq of all major immune cell types	Yoshida et al.[92]	GEO: GSE100738
Bulk RNA-seq of macrophages from MC38 tumors	Wang et al.[93]	GEO: GSE185591
Bulk RNA-seq of the 12 macrophage populations	Qie et al.[55]	SRA: PRJNA482293
ATAC-seq of peritoneal macrophages	Lavin et al.[46]	GEO: GSE63338
Bulk RNA-seq of peritoneal MFs	This paper	GEO: GSE254406
RXRα ChIPmentation data	This paper	GEO: GSE254407
scRNA-seq of peritoneal MFs	This paper	GEO: GSE254572
Bulk RNA-seq of converting MFs	This paper	GEO: GSE273340
Experimental Models: Cell lines		
Lenti-X™ 293T Cell Line	TaKaRa	Cat# 632180
Experimental Models: Organisms/Strains		
Mouse: C57BL/6J	Jackson Laboratory	JAX# 000664
Mouse: BALB/c	Jackson Laboratory	JAX# 001026
Mouse: CD45.1: B6.SJL-*Ptprc*^{a} *Pepc*^{b}/BoyJ	Jackson Laboratory	JAX# 002014
Mouse: Cas9 knockin: B6J.129(Cg)-Gt(ROSA)26Sor$^{tm1.1(CAG-cas9*,-EGFP)Fezh}$/J	Jackson Laboratory	JAX# 026179
Mouse: B6.Kaede mice	Tomura et al.[94]; Morton et al.[95]	N/A
Mouse: B6.*Foxp3*-IRES-*Thy1.1*	Liston et al.[96]	N/A
Mouse: *Nlrp3*$^{-/-}$: B6.129S6-*Nlrp3*^{tm1Bhk}/J	Jackson Laboratory	JAX# 021302
Mouse: *Casp1*$^{-/-}$:B6N.129S2-*Casp1*^{tm1Flv}/J	Jackson Laboratory	JAX# 016621

(*Continued on next page*)

Please cite this article in press as: Wang et al., A pan-family screen of nuclear receptors in immunocytes reveals ligand-dependent inflammasome control, Immunity (2024), https://doi.org/10.1016/j.immuni.2024.10.010

Continued

REAGENT or RESOURCE	SOURCE	IDENTIFIER
Mouse: *Gsdmd*$^{-/-}$: C57BL/6N-*Gsdmd*^{em4Fcw}/J	Jackson Laboratory	JAX# 032410
Mouse: B6 Asc$^{-/-}$	Hise et al.[97]	N/A
Mouse: *GATA6*$^{fl/fl}$: B6.*Gata6* $^{tm2.1Sad/J}$	Jackson Laboratory	JAX# 008196
Mouse: *LysM*-cre: B6.129P2-*Lyz2* $^{tm1(cre)Ifo}$/J	Jackson Laboratory	JAX# 004781
Mouse: *Cd115*-ERcre: B6.FVB-Tg(Csf1r-cre/Esr1*)1Jwp/J	Jackson Laboratory	JAX# 019098
Oligonucleotides		
gRNA oligo sequence	This paper (Table S1)	N/A
Primers for amplicon sequencing	This paper (Table S1)	N/A
Recombinant DNA		
pLKO.3G-EGFP-Filler	This paper	N/A
pLKO.3G-mcherry-Filler	This paper	N/A
pLKO.3G-BFP-Filler	This paper	N/A
psPAX2	Addgene	Addgene Cat# 12260
VSV-G	Addgene	Addgene Cat# 138479
pMSCV-IRES-GFP-mouse-Caspase-1	Addgene	Addgene Cat# 183361
pCDNA3.1-HA-mouse-ASC	This paper	N/A
pCDNA3.1-Flag-mouse-RARγ	This paper	N/A
Software and algorithms		
HOMER v4.9	Heinz et al.[98]	http://homer.ucsd.edu
t- SNE	van der Maaten and Hinton[99]	https://lvdmaaten.github.io/tsne/
ImageJ1 version 2.9.0	FIJI software	https://imagej.net/ij/download/
Prism10	GraphPad	https://www.graphpad.com/scientificsoftware/prism/
FlowJo 10	FlowJo, LLC	https://www.flowjo.com
IGV v2.4.14	Robinson et al.[100]	https://software.broadinstitute.org/software/igv/
BEDTools v2.27.1	Quinlan and Hall[101]	https://bedtools.readthedocs.io
Bowtie 2 v2.3.4.3	Langmead and Salzberg[102]	https://github.com/BenLangmead/bowtie2
Trim Galore	The Babraham Institute	https://github.com/FelixKrueger/TrimGalore
Picard v2.8.0	Broad Institute	https://broadinstitute.github.io/picard/
Chrom VAR v1.4.1	Schep et al.[103]	https://github.com/GreenleafLab/chromVAR
R v4.1.0	R Core Team	https://www.r-project.org/
Seurat v4.0.2	Hao et al.[104]	https://satijalab.org/seurat/
MACS v2.1.1	Zhang et al.[105]	https://github.com/macs3-project/MACS
deep Tools v3.0.2	Ramirez et al.[106]	https://deeptools.readthedocs.io/en/3.0.2/index.html
SAMtools v1.3.1	Li et al.[107]	https://www.htslib.org/
Morpheus	Broad Institute	https://software.broadinstitute.org/morpheus/
STAR v2.7.3a	Dobin et al.[108]	https://github.com/alexdobin/STAR
FeatureCounts (Subread v2.0.0)	Liao et al.[109]	https://subread.sourceforge.net/
DESeq2 v1.28.1	Love et al.[110]	https://github.com/thelovelab/DESeq2
RSeQC v2.6.4	Wang et al.[111]	https://rseqc.sourceforge.net/
CRISPResso2	Clement et al.[112]	https://github.com/pinellolab/CRISPResso2

(*Continued on next page*)

Please cite this article in press as: Wang et al., A pan-family screen of nuclear receptors in immunocytes reveals ligand-dependent inflammasome control, Immunity (2024), https://doi.org/10.1016/j.immuni.2024.10.010

Continued

REAGENT or RESOURCE	SOURCE	IDENTIFIER
Other		
Vitamin A deficient diet	Envigo Teklad Diets	TD.09838
Vitamin A control diet	Envigo Teklad Diets	TD.09839
BD Symphony A5	BD Biosciences	N/A
Aria II (561)	BD Biosciences	N/A
MoFlo Astrios	Beckman Coulter	N/A
Aurora spectral analyzer	Cytek Biosciences	N/A
Leica Thunder microscope	Leica Microsystems	N/A

METHOD DETAILS

Mice

C57BL6/J (JAX strain # 000664), BALB/c (JAX strain # 001026), congenic CD45.1 strain (C57BL/6J background, JAX strain # 002014), Rosa26-*Cas9* knock-in mice (JAX strain #026179),[113] *Foxp3*-IRES-*Thy1.1* reporter mice,[96] *Nlrp3*$^{-/-}$ mice (JAX strain # 021302),[114] *Casp1*$^{-/-}$ mice (JAX strain# 016621),[115] *Gsdmd*$^{-/-}$ mice (JAX strain # 032410),[116] *Asc*$^{-/-}$ mice (Millennium Pharmaceuticals),[97] *Gata6*$^{flox/flox}$ mice (JAX strain # 008196), *LysM*-cre (JAX strain # 004781) and *Cd115*-ERcre mice (JAX strain # 019098)) were bred in our facilities at HMS, BCH, UMCMM or WashU. Rosa26-*Cas9* knock-in mice were crossed with *Foxp3*-IRES-*Thy1.1* reporter mice to generate *Cas9*/*Foxp3*$^{thy1.1}$ mouse line. *Gata6*$^{flox/flox}$ mice were crossed to *Lysm*-cre (JAX strain # 004781) and *Cd115*-ERcre mice (JAX strain # 019098)) to generate cell-specific GATA6 deficiencies mice.[47] To induce recombinase activity, *Cd115*-ERCre × *Gata6*$^{flox/flox}$ × Rosa26TdTomato mice and *Gata6*$^{flox/flox}$ × Rosa26TdTomato littermate controls were received 2 mg tamoxifen (100 μL of a 20 mg/mL stock solution, diluted in corn oil) by oral gavage every other day for a total of three doses. Mice were analyzed one week after the last dose. Mice were generally used for experiments between 6-8 weeks of age. Both male and female mice were used for experiments, after confirming no difference between sexes. All mice were bred and maintained in specific pathogen free conditions at Harvard Medical School. All experiments were performed following guidelines listed in animal HMS Institutional Animal Care and Use Committee protocols IS00000196 and IS00001257 and Washington University protocol 22-0433.

Vitamin A depletion

C57BL/6 mice were bred with either a vitamin A deficient diet (Harlan, TD.09838) or control diet containing vitamin A (20000IU/kg diet in the TD.09838), beginning at 13.5 days of gestation. The pups were weaned at 3 week of age and maintained on the same diet until analysis was performed.

NR ligand treatments

6- to 8-week-old cohoused C57BL/6 mice were used. The agonist and antagonist compounds were injected i.p., as specified in Table S6. For LPS, mice were injected i.p. with 10 μg LPS (Sigma-Aldrich, L-2880) in 100 μl PBS (at 0.5 mg/kg weight). Controls from the same lots of mice were injected with PBS.

Cell isolation and flow cytometry

Mice were euthanized with CO2 and perfused with 30 mL PBS. Spleen, liver, lung, epididymal VAT and colon samples were collected, minced, and digested at 37°C with shaking as follows:

Spleen

Splenic myeloid cells were released by enzymatic digestion in 5 mL phenol red-free Dulbecco's Modified Eagle Medium (DMEM) (Gibco) containing 2% fetal calf serum (FCS),1 mg/mL Collagenase IV (Gibco) and 10 U/mL DNaseI (Sigma) for 20 min. Splenic lymphocytes were released using mechanical dissection.

Peritoneal lavage cells

8 mL sterile PBS containing 2% FCS and 2 mM EDTA was injected into the peritoneal cavity. A massage was applied to the abdomen prior to abdominal incision and collection of the fluid. LPMs were purified by sorting CD11b^{hi}F4/80^{hi} cells using a BD-Aria sorter. To obtain thioglycolate elicited peritoneal macrophages (TGEMs), mice were injected i.p. with 2 mL 3% sterile thioglycolate. After 2 days, TGEMs were collected using peritoneal lavage.

Lung and liver

Liver and lung were digested in 25 mL RPMI containing 0.5 mg/mL collagenase IV (Gibco) and 0.05 mg/mL DNase I (Sigma) for 40 min. The liver immune cells were subsequently purified through a 33% Percoll (GE Healthcare) gradient centrifugation using 30 mL of PBS containing 2% FCS, 15.3 mL of neat Percoll, and 1.7 mL of 10 x PBS for 10 min at 800x g.

VAT

Epididymal visceral adipose tissue (VAT) was digested in 5 mL DMEM containing 2% FCS and 1.5 mg/mL collagenase type II (Sigma) for 20 min.

Please cite this article in press as: Wang et al., A pan-family screen of nuclear receptors in immunocytes reveals ligand-dependent inflammasome control, Immunity (2024), https://doi.org/10.1016/j.immuni.2024.10.010

Colon

The entire colon was incubated in RPMI (Gibco) containing 2% FCS, 1 mM DTT and 20 mM EDTA at 37°C for 15 min to remove epithelial cells. The colon was then minced and dissociated in RPMI containing 1% FCS, 1.5 mg/mL collagenase II (Gibco), and 0.5 mg/mL Dispase (Gibco) at 37°C for 40 min, with constant stirring.

MC38 tumor induction and cell isolation

MC38 cells were cultured in DMEM supplemented with 3 mM L-Glutamine and 100 U/mL penicillin-streptomycin. On day 20 after bone marrow reconstitution, each BMC mouse was subcutaneously inoculated on the abdomen with one million MC38 cells in 100 μL PBS. On day 17 after MC38 cell inoculation, solid tumor tissues were isolated, then chopped, and digested in DMEM containing 2% FCS, 1 mg/mL collagenase type IV (Gibco), and 20 μg/mL DNAse I (Sigma) at 37°C for 20 min with shaking.

For all tissues, the digested materials were lysed using ACK lysis buffer (Gibco) to remove red blood cells and then filtered through a 40 μm cell strainer to get single cell suspensions. Cells were stained with different antibody panels as detailed in experimental descriptions or "Rainbow-CRISPR" screen section. For surface-antigen staining, single-cell suspensions were incubated in phosphate-buffered saline (PBS) containing live/dead stain and surface antibodies for 15 min on ice, followed by washes in 2%FCS DMEM buffer. For intracellular staining, cells were fixed in eBioscience Fix/Perm buffer for 30 min at room temperature, followed by permeabilization in eBioscience permeabilization buffer at room temperature for 60 min in the presence of intracellular antibodies. For Annexin V and propidium iodide (PI) staining, cells were incubated with 5 μL of PE- or APC- conjugated Annexin V (Biolegend) in 100 μL of Annexin V binding buffer (Biolegend) at room temperature for 10 min. Then 2 μg/mL of PI (Sigma) was then added to each sample and incubated for another 5 min. After that, 500 μL of Annexin V binding buffer was added to the cells for washing. The cells were either analyzed immediately or fixed in 1% formaldehyde for 10 min before flow cytometry analysis with BD FACSymphony or Cytek Aurora.

Rainbow-CRISPR screen

Guide RNA design and cloning

The gRNA lentiviral vector was modified from pLKO.3G (Addgene # 14748) by introducing the U6 promoter-filler-gRNA scaffold-cPPT-PGK promoter fragment. EGFP was replaced with either BFP or mCherry, to generate different fluorescent reporters. The gRNAs (listed in Table S1A) were designed using CRISPick software[117,118] from the Broad Institute. Three gRNAs were selected for each NR. Non-targeting control gRNAs were picked from the GeCKO v2 mouse library.[119] The intergenic control gRNAs targeting murine safe harbor genome locations were picked from the genome-wide gRNA library.[120] All guide RNA oligos with BsmBI-compatible overhangs were purchased from IDT, and annealed, phosphorylated, and cloned into the gRNA lentiviral vector by BsmBI restriction digestion as described.[119]

Lentivirus production and titration

Lentivirus was packaged using HEK293T cells (TaKaRa). Briefly, cells are split and seeded into a 6-well plate to reach ~80% confluence before transfection. Three gRNA expressing lentiviral plasmids targeting the same NR were mixed equally and co-transfected with package plasmids psPAX2 and VSVG at a ratio of 2:1:1 using TransIT-293 reagent (Mirus Bio, MIR2704) following the manufacturer's instructions. The virus-containing supernatant was collected 48 h after transfection and filtered through a 0.45 μm syringe filter. Lentivirus was concentrated using PEG-it lentivirus concentration reagent (System Biosciences) following the manufacturer's instructions. Virus titers were quantified by infecting HEK293T cells with serial dilutions of the virus. Infected cells were detected by recording BFP-, EGFP-, or mCherry-positive cells using flow cytometry. The viral titer was then calculated using the formula: Titer in pfu/mL = ((# of cells at start time) * (dilution factor) * (percent of infection)) / (volume of virus solution added). An infection rate of 1~10% was used.

Bone marrow isolation and bone marrow chimera generation

Bone marrow cells were isolated from the tibia and femur of the Cas9/Foxp3$^{thy1.1}$ mice, flushed and ACK-lysed. After depleting the Lineage$^+$ populations with biotinylated antibodies (anti-CD4, CD8, CD11b, CD11c, CD19, Gr1, NK1.1, Ter119) and Dynabeads Biotin Binder (Thermo Fisher Scientific) following the manufacturer's instructions, LSK cells (Lineage$^-$c-Kit$^+$Sca-1$^+$) were sorted using Aria 561 sorter. The purified LSK cells were cultured overnight in StemPro-34 SFM (Gibco) complete medium containing 1x Supplement, 2mM L-glutamine and 100 ng/mL recombinant murine cytokines (e.g., SCF, Flt3 ligand, IL-7, and TPO (all from PeproTech)). The following day, the LSK cells were transduced with different gRNA lentiviruses at MOI=20 through spin-transduction on a RetroNectin-coated plate at 650x g for 90 min. In the "Rainbow-CRISPR" screen, each bone marrow chimera (BMC) mouse received a mixture of three LSK populations, identifiable by different fluorescent reporters (BFP, EGFP, and mCherry). One was transduced with a control -targeting gRNA virus and served as the internal control, while the other two populations were transduced with gRNA lentiviruses targeting a given NR. In practice, each targeting actually used simultaneously 3 different gRNAs against the same gene, with same fluorescent reporter. In addition, to guard against an effect of the double-stranded breaks created in the HSCs, we used gRNAs inducing breaks in "safe harbor" loci. The three LSK populations were mixed equally and transferred into irradiated CD45.1$^+$ recipients through retro-orbital injection 24 h post virus transduction. After allowing for reconstitution and differentiation to proceed (4 weeks for myeloid cells, 10 weeks for T and B cells), cells were isolated from spleen and peritoneal lavage, prepped, and stained for flow analysis.

Immunophenotyping by flow cytometry

Single cell suspensions were stained with four constant panels of antibodies: 1) splenic myeloid panel contains antibodies against CD45.2, CD19, CD11b, CD11c, F4/80, MHCII, Ly6C, Ly6G, CD8a and PDCA1; 2) peritoneal myeloid panel contains antibodies

against CD45.2, CD19, CD11b, F4/80,Ly6C, Ly6G and Siglec-F; 3) splenic B cell panel contains antibodies against CD45.2,CD19, TCRβ, IgM, IgD, CD23, CD93, CD21/35, CD138, Fas and CD38; 4) splenic T cell panel contains antibodies against CD45.2, CD19, TCRβ, TCRγδ, CD4, CD8a, CD90.1 (thy1.1), CD44 and CD62L (see detailed gating strategies in Figures S2B–S2E). To maintain data consistency, the antibodies were kept at a constant concentration, clone, and source. The gRNA frequencies in each immune cell-type were quantified by flow analysis of BFP/GFP/mcherry expression using Cytek Aurora.

Immunophenotyping data normalization and statistical analysis

Screen data were obtained from at least two independent experiments, each using a distinct batch of gRNA lentiviruses and BMC mice. The entire set of data were analyzed by FlowJo Software. Data with strong discrepancies in staining caused by reagent drift (e.g., enzymes and antibodies, etc.), or with low quality such as those with a low number of plasma B cells, or those that involved unclear gating of fluorescent protein in γδT cells, were excluded from the analysis. A total of 35 NRs across 28 cell types were included in the data set, all of which exhibited high-quality flow data.

Data processing involved one or more normalization steps, to correct for the inherent variability in such experiments (variable organ sizes and cell counts in BMC mice, different levels of engraftment, fluctuations in lentiviral titers), exploiting the control-gRNA-transduced cells differentiating in the same mouse (as ratios of the fluorescence reporters carried by the lentiviruses), as well as the relative frequencies of differentiated cell edited by a particular gRNA relative to the whole population carrying this guide in the same mouse (for instance, normalizing the ratio relative to Ctrl observed in Treg cells to the same ratio in total T cells in the same mouse).

For Figure 1B, the NR/Ctrl ratio in total donor-derived $CD45^+$ cells was calculated (frequency of cells carrying targeting gRNA vs frequency of cells carrying control gRNA in the same mouse) (see Table S1D for details), with significance tested by a one-sample t test (vs null hypothesis with this ratio= 1). In other panels, which analyze the effect of NRs on differentiated cells, the NR/Ctrl ratio of each immunological cell type was normalized to the NR/Ctrl ratio of the total donor-derived $CD45^+$ cells carrying the same gRNA, or all B, or all αβT cells in the same BMC host. Changes in cell types that constitute a dominant proportion of cells within a compartment may artefactually induce apparent changes in other cell types (in particular, changes in large peritoneal macrophages alter the proportion of peritoneal B cells). To circumvent this issue, we normalized the NR/Ctrl ratio of peritoneal cell types to the NR/Ctrl ratio of total donor-derived $CD45^+$ splenocytes in the same BMC host (see Table S1E for details). Statistical analysis was assessed by one-way ANOVA with Dunnett correction.

CRISPR editing frequency quantification by amplicon sequencing

The efficacy of gRNA editing was assessed by amplicon sequencing around the gRNA target sites, in both the HSC population prior to transfer and in recovered B lymphocytes, by pooled amplicon sequencing of target regions using the Illumina MiSeq platform. Briefly, on day 3 following lentivirus transduction, LSK cells with NR mutations were sorted. B cells with NR mutations were sorted from BMC mice at 10 weeks after reconstitution. Genomic DNA was extracted from the sorted cells using Arcturus PicoPure DNA Extraction Kit (ThermoFisher Scientific) and amplicon libraries were prepared by employing a 2-step PCR method using NEBNext High-Fidelity 2x PCR Master Mix (New England Biolabs). Locus-specific primers flanking the modification site and containing universal 5′ tails with partial Illumina adapters were designed (primers listed in Table S1B). The modification site should be close to the center of the amplicon fragment and ideally at least 50 bp away from the primer-binding sites. In step1 PCR, locus-specific primers are used to amplify the genomic regions containing modification sites. In step2 PCR, the amplicons from step 1 were introduced with the remaining Illumina sequencing adaptor and sample barcodes (primers listed in Table S1B). Samples were prepared for Illumina MiSeq according to the manufacturer's instructions with unique barcode for each cell type. Data were analyzed using CRISPResso2 with the default parameters as previously described.[112] CRISPResso2 aligns sequencing reads to a reference sequence and quantifies insertions, mutations, and deletions to determine whether a read is modified or unmodified by genome editing. Editing frequency was calculated as the percentage of reads containing a frame-shift indel out of total reads at each target site (see Table S1C). The code available at https://github.com/CBDM-Lab/NR-screen-Homozygote-Frequency was used to calculate the frequency of cells carrying one or more homozygous knockout mutation of the target gene.

Population (ULI) RNA-seq

Cell sorting

RNA-seq was performed on purified peritoneal MFs sorted from "Rainbow-CRISPR" mice 4 weeks after reconstitution, each mouse yielding two NR mutant samples and one control (for economy, only 12 Ctrl samples were profiled overall). Biological duplicates were obtained for each NR ablation, sorted on different days to reduce batch effects. The standard ImmGen ULI-RNA-seq protocol (http://www.immgen.org/), on 1,000 double-sorted cells – second sort directly into 5 μL TCL (Qiagen) lysis buffer containing 1% 2-mercaptoenthonol (Sigma). NR-deficient peritoneal MFs were sorted by their corresponding gRNA-conjugated fluorescence reporter, as live $CD19^-CD11b^{hi}F4/80^{hi}$.

Library preparation

Multiple wild-type samples were sorted and paired with NR-deficient cells on the same day. Smart-seq2 libraries were prepared by Broad Technology Labs following previously described protocol with slight modifications.[121,122] Briefly, total RNA was captured and purified using RNAClean XP beads (Beckman Coulter). Polyadenylated mRNA was then selected using an anchored oligo (dT) primer (50-AAGCAGTGGTATCAACGCAGAGTACT30VN-30) and converted to cDNA via reverse transcription. First-strand cDNA was subjected to limited PCR amplification followed by transposon-based fragmentation using the Nextera XT DNA Library Preparation Kit

(Illumina). Samples were then PCR amplified for 12 cycles using barcoded primers such that each sample carries a specific combination of eight base Illumina P5 and P7 barcodes and pooled together prior to sequencing. Smart-seq paired-end sequencing is performed on an Illumina NextSeq500 (two full NextSeq runs per batch of 96 samples, for 10 million raw reads/sample on average) using 2 x 38 bp reads with no further trimming.

Data preprocessing and quality control

Reads were aligned to the mouse genome (GENCODE GRCm38/mm10 primary assembly and gene annotations vM25; https://www.gencodegenes.org/mouse/release_M25.html) with STAR 2.7.3a[108] The ribosomal RNA gene annotations were removed from GTF (General Transfer Format) file. The gene-level quantification was calculated by featureCounts (http://subread.sourceforge.net/). Raw reads count tables were normalized by median of ratios method with DESeq2 package from Bioconductor[110] and then converted to.gct and.cls format.

Samples with less than 1 million uniquely mapped reads, or having less than 8,000 genes with >10 reads, or with transcript integrity number (TIN) < 45 were removed from the data set prior to downstream analysis and excluded from normalization to mitigate the effect of poor-quality samples on normalized counts. In addition, biological replicates were analyzed for Pearson correlation to identify poor-quality samples and remove them from the data set. Pearson correlation was calculated on transcripts with an average of > 5 reads or below the 99th percentile for number of reads in the dataset to avoid outlier effects. Any replicates that did not exhibit a correlation of 0.9 or greater were removed from the data set prior to downstream analysis. Finally, the RNA integrity for all samples was measured by median transcript integrity number (TIN) across mouse housekeeping genes with RSeQC ('tin.py', v2.6.4).[111]

Analysis of NR-affected transcripts

To eliminate noise from transcripts with low expression levels, genes were retained for consideration if they had an expression >20 in at least one condition. Some genes yield intrinsically high variance even in wild-type dataset. These "noisy" genes were removed from consideration if their 90th percentile of inter-replicate coefficient of variation across all the mutants was > 0.75. A FoldChange matrix was generated for each mutant sample relative to the Ctrl samples prepared on the same sorting date. A 1-sample t-test was performed to determine whether FCs for each NR mutant are different from 1. Potential differentially expressed (pDE) genes for each NR mutant were identified by FC < 0.5 or FC >2 and nominal t.test p-value < 0.05. The final set of pDE genes was the union of all the pDE genes from each NR mutant. The expression heatmap was generated with Morpheus (https://software.broadinstitute.org/morpheus).

scRNA-seq analysis of peritoneal macrophages

Cell sorting and pooling using cell hashtagging

Information on BMC mice and corresponding hashtags was detailed in Table S4A. Peritoneal exudate cells extracted from each BMC mouse were stained in 100 μL of FACS buffer (phenol red-free DMEM, 2% FCS, 0.1% azide and 10 mM HEPES, pH 7.9) containing 10 μL FcBlock (homemade), CD11b APC (1 μL, M1/70, BioLegend), and CD115 PE/Cy7 (1 μL, AFS98, BioLegend), 1 μL (0.5 μg) of a unique hashtag antibody for 10 min. Wild-type and four different NR mutants, including RARγ mutant, RXRα mutant, RORα mutant, and RXRβ mutant were sorted by their corresponding gRNA-conjugated fluorescence reporter, as live CD11b^{+}CD115^{+} cells into PBS–BSA 0.1% medium using the Aria561 cell sorter (70-μm nozzle). Each NR mutant has two replicates, while three wild-type samples were paired with NR mutant cells from the same BMC mouse. Samples of the same genotype were combined and hashtagged again. The multiple hash-tagged samples (46,000 cells in total) were then combined into one tube with a final volume of 30 μL PBS-BSA 0.1%. The single-cell RNA-Seq libraries were prepared using the 10X Genomics Single Cell 3′ Reagent kit (V3 chemistry) following the manufacturer's protocols.

Hashtag libraries

Hashtag libraries were made separately as described.[123] In brief, at the cDNA amplification step in the Single Cell 3′ Reagent kit protocol, the yield of HTO (Hashtag Oligo) products was increased using an 'additive' primer to cDNA PCR. Hashtag-derived cDNAs (<180 bp) and mRNA-derived cDNAs (>300 bp) were then separated using 0.6× SPRI bead selection. The supernatant contained the hashtag-derived cDNA that was purified with two rounds of 2× SPRI beads. The sequencing oligonucleotides were added by PCR which also amplified the Hashtag library. Libraries were sequenced on the NextSeq 500 platform (28/8/0/91, Read1/i7/i5/Read2). Hashtag count matrices were obtained from CITE-Seq-Count package (https:// zenodo.org/record/2590196).

scRNA-seq analysis

scRNA-seq data were processed using the standard CellRanger pipeline (10x Genomics). HTO counts were obtained using the CITE-seq-Count package. Processed matrix, barcodes and feature files were loaded in R (v4.3.1) using Seurat (v5.0.1). Hashing data were used to classify each cell based on the predominant dual hashtag configuration. Cells with fewer than 500 reads or with greater than 10% of reads mapped to mitochondrial genes were excluded from the analysis. Dimensionality reduction, visualization, and clustering analysis were performed in Seurat using the NormalizeData, ScaleData, FindVariableGenes, RunPCA, FindNeighbours, RunUMAP (dims = 1:15), and FindClusters (res = 0.7) functions. The method returned 12 cell clusters which were then visualized using UMAP for dimensionality reduction. Clusters 11 (T cells) and 12 (B cells) where minor contaminants that were removed using the SubsetData function. Cluster identity was determined on the basis of expression of key marker genes (Figures 4B and S4B). DE genes in each cluster were determined by FindAllMarkers and FindMarkers.

Chromatin immunoprecipitation (ChIPmentation)

Library preparation

ChIPmentation libraries were prepared following the protocol as described[124] with some modifications. In brief, approximately 100,000 LPMs per sample were sorted from peritoneal exudate cells of 8-week-old C57BL/6 mice. Briefly, cells were fixed with 1% fresh formaldehyde (Thermo Fisher Scientific) for 10 min at room temperature with rotation, followed by quenching using 0.125 M glycine for 5 min. After washing with ice-cold PBS supplemented with cOmplete protease inhibitor (Roche), cells were resuspended in lysis buffer (10 mM Tris-HCl pH 8.0, 2 mM EDTA, 0.25% SDS, 1x protease inhibitor), and sonicated on the Covaris M220 ultra-sonicator to obtain 200-300 bp DNA fragments using the following settings: peak incident power 50, duty factor 10%, cycles per burst 200, time 8 min. Keep 2 μL of supernatant from two replicates as the input DNA at -20 °C. The remaining supernatant was incubated overnight at 4°C on a rotator with 3 μg of anti-RXRα (D6H10) Rabbit mAb (#3085, Cell Signaling) pre-coupled to Protein A Dynabeads (Invitrogen). The beads were washed twice sequentially on a pre-cold magnet (Invitrogen) using RIPA-LS wash buffer (10mM Tris-HCl pH 8.0, 140 mM NaCl, 1 mM EDTA, 0.1% SDS, 0.1% sodium deoxycholate, 1% Triton X-100), RIPA-HS wash buffer (10mM Tris-HCl pH 8.0, 500 mM NaCl, 1 mM EDTA, 0.1% SDS, 0.1% sodium deoxycholate, 1% Triton X-100), and RIPA-LiCl wash buffer (10 mM Tris-HCl pH 8.0, 250 mM LiCl, 1mM EDTA, 0.5% NP-40, 0.5% sodium deoxycholate) and followed by a wash with 10 mM Tris-HCl pH 8.0. After washing, the beads were then resuspended in 25 μL tagmentation reaction mix containing 1 μL Tn5 transposase (Illumina), and incubated at 37°C for 5 min. After removing the tagmentation reaction mix, beads were washed twice with RIPA-LS wash buffer and once with TE buffer (10 mM Tris-HCl pH 8.0, 500 mM EDTA), followed by elution with 48 μL elution buffer (10 mM Tris-HCl pH 8.0, 300 mM NaCl, 5 mM EDTA, 0.4% SDS) containing 2 μL Proteinase K (NEB) at 55°C for 1 h and 65°C for 8 h for de-crosslinking. The input DNA was also incubated with tagmentation reaction mix, and de-crosslinked with Proteinase K. DNA was purified using MinElute Reaction Cleanup Kit (QIAGEN). Libraries were indexed and amplified using the NEBNext High-Fidelity 2x PCR Master Mix (NEB) and ATAC-seq primers,[125] followed by purification using AMPure XP beads (BeckmanCoulter) and sequencing as for ATAC-seq.

ChIPmentation data analysis

After removing adapters and low-quality reads using Trim Galore (https://github.com/FelixKrueger/TrimGalore), we aligned ChIP-seq reads to the corresponding genome (mm10 reference genome) by Bowtie 2[102] with the following parameters: -X 1000 –fr –no-mixed –no-discordant. Nonuniquely mapped and mitochondrial DNA reads were removed using a combination of SAMtools functions.[107] PCR duplicates were removed using Picard ('MarkDuplicates', v2.8.0, https://broadinstitute.github.io/picard/). ChIP-seq peaks for individual samples were identified using MACS2[105] ('callpeak', v2.1.1.20160309) with the following parameters: –keep-dup all –nomodel –shift -100 –extsize 200 -p 0.05. High-confidence, reproducible ChIP-seq peaks among replicates were then identified with a global FDR < 0.01. Peaks overlapping the suspect list of problematic regions[126] were removed from downstream analyses using BEDTools (v2.27.1)[101] To visualize individual ChIP-seq tracks using the Integrative Genomics Viewer (IGV, v2.4.14)),[100] the alignment file (BAM file) was converted to the read-coverage file (BigWig file) using deepTools[127] ('bamCoverage', v3.0.2). The peak annotation was performed using HOMER[98] ('annotatePeaks.pl', v4.9) (binding peaks listed in Table S6).

TF motif enrichment

Motif enrichment analysis for RXRα binding peaks were performed using findMotifsGenome.pl with the default parameters from HOMER.

In vitro cell treatments

The FACS-purified LPMs were resuspended in DMEM F12 medium (Gibco) supplemented with 10% FBS, 3 mM L-Glutamine and 100 U/mL penicillin-streptomycin and seeded in 24-well plate. After cell adhesion for 1 h, cells were washed twice with PBS and stimulated with indicated stimuli in Opti-MEM (Gibco) specified in the figure legends.

To evaluate the effect of RARγ antagonist LY2955303 on cell death programs, LPMs were left untreated or treated with 50 μM LY2955303 (Tocris) alone, or in combination with pretreatment of 200 μM Lonidamine (Tocris, LND, ASC inhibitor), 25 μM VX765 (Tocris, caspase-1 inhibitor), or 2 μg/μL of the cOmplete protease inhibitor cocktail (Roche) for 1 h prior to LY treatment.

To assess the effect of RARγ agonist BMS961 on inflammasome activation, LPMs were either left untreated or treated with 30 μM BMS961 (Tocris) for 1 h prior to exposure to inflammasome ligands. For NLRP3 inflammasome, B6 LPMs were primed with 500 ng/mL LPS (Sigma-Aldrich, L-2880) for 3 h followed by stimulation with 10 mM nigericin or 5 mM ATP for 30 min. For AIM2 inflammasome, LPS-primed B6 LPMs were transfected with 2 μg poly(dA:dT) for 6 h using Lipofectamine 3000 (Invitrogen, L3000001). For NLRC4 inflammasome, LPS-primed B6 LPMs were infected for two h with wildtype Shigella 2457T which was grown as previously described.[128] Briefly, an overnight culture of *Shigella* 2457T was back-diluted into 5 mL of TCS (trypticase soy) broth and incubated at 37°C for 2 h with shaking. The culture was pelleted and resuspended in Opti-MEM and spun onto cells for 10 min at 300xg at an MOI of 30. Infected cells were incubated at 37°C in a 5% CO_2 incubator for 20 min and then washed for three times with Opti-MEM containing 50 μg/mL gentamicin, then returned to 37°C for further incubation for 100 min. For NLRP1b inflammasome, LPMs from BALB/c mice that express NLRP1b were treated with different concentrations of anthrax lethal toxin (LeTx) for three h. The low dose consisted of 2 μg/mL protective antigen (PA) and 1 μg/mL lethal factor (LF), while the high dose comprised 10 μg/mL PA and 10 μg/mL LF. Cells were pretreated and maintained in vehicle or 30 μM BMS961 throughout the experiment. After cell treatment, IL-1β secretion and LDH secretion was measured in the supernatants by Lumit™ IL-1β mouse immunoassay kit (W7010, Promega)

Please cite this article in press as: Wang et al., A pan-family screen of nuclear receptors in immunocytes reveals ligand-dependent inflammasome control, Immunity (2024), https://doi.org/10.1016/j.immuni.2024.10.010

and LDH-Glo™ Cytotoxicity Assay (J2380, Promega) according to the manufacturer's instructions. The cells together with the culture supernatants (in Opti-MEM) were lysed with 5 x SDS for immunoblotting analysis.

Immunoblotting and protein analysis

Western blotting

After cell treatment, the cells and culture supernatants were lysed in 5x SDS sample loading buffer containing 50% glycerol, 10% SDS, 5% 2-mercaptoethanol, 0.02% bromophenol blue, 250 mM (pH 6.8) Tris-HCl, and cOmplete protease inhibitors (Roche). The proteins were separated by 8%–12% SDS-PAGE and electrophoretically transferred to PVDF membranes (Millipore IPVH00010). After blocking non-specific binding with 5% skim milk, the membranes were incubated overnight with indicated primary antibodies: anti-caspase-1 (AG-20B-0044, AdipoGen), anti-caspase-3 (#9662,CST), anti-cleaved caspase-3 (#9661, CST), anti-caspase-7 (sc-56063,Santacruz),anti-caspase-8(sc-81656,Santacruz),anti-GSDMD (sc-393581, Santacruz), anti-GSDMD (ab209845, Abcam), anti-GATA6 (sc-518050, Santacruz), anti-PARP (# 9542,CST), anti-ASC(#67824, CST), anti-NLRP3 (AG-20B-0014-C100, AdipoGen) and anti-GAPDH (ab9484, Abcam). Membranes were then washed and probed with corresponding horseradish peroxidase (HRP)–conjugated secondary antibodies (from Jackson ImmunoResearch Laboratories): donkey anti-mouse IgG (H+L) (#715-035-150), goat anti-rabbit IgG (H+L) (#111-035-144), and goat anti-mouse IgG, light chain specific (#115-035-174). Immunoblot images were acquired by Image Lab software (Bio-Rad) using SuperSignal™ West Femto Maximum Sensitivity Substrate (#34094, Thermo Fisher Scientific).

Co-immunoprecipitation

For endogenous immunoprecipitation, C57BL/6 mice were i.p. injected with either vehicle or 50 nmoles LY2955303 for 10 min (n=5 mice per group). Total peritoneal cells were collected and resuspended in 1mL ice-cold lysis buffer (20 mM Tris-HCl (pH 7.4), 150 mM NaCl, 1% Triton X-100, 10% glycerol, 1 mM Na_3VO_4, 2 mM PMSF, EDTA-free protease inhibitor cocktail) and incubated on a rocker at 4 °C for 1 h. After centrifugation at 20,000 X g, 4 °C for 10 min, collect 50 μL lysate as the whole cell lysate. The remaining lysates were incubated overnight at 4°C on a rotator with 3 μg IgG control antibody (#2729, Cell Signaling), or anti-RARγ antibody (11424-1-AP, Proteintech) or anti-RARγ (sc-7387, Santacruz) antibody pre-coupled to Protein A Dynabeads (Invitrogen). Subsequently, the beads were then washed three times with lysis buffer and boiled in 2 x SDS loading buffer at 100 °C for 5 min.

For immunoprecipitation in the overexpression system, HEK293T cells were seeded into six-well plates and transfected with the indicated combination of pCDNA3.1-Flag-mouse-RARγ, pMSCV-IRES-GFP-mouse-Caspase-1 (#183361, Addgene), or pcDNA3-HA-mouse-ASC plasmids for 24 h. Cells were then collected and lysed in an ice-cold lysis buffer (50 mM Tris-HCl (pH 7.4), 150 mM NaCl, 1mM EDTA, 1% Triton X-100, 10% glycerol, 0.02% digitonin, 2 mM PMSF, protease inhibitor cocktail). The lysates were incubated overnight with prewashed Anti-FLAG® M2 Magnetic Beads (M8823, Sigma-Aldrich). Subsequently, the beads were then washed three times with lysis buffer and boiled in 2 x SDS loading buffer at 100 °C for 5 min. The immunoprecipitated and input samples were subjected to immunoblotting analysis and stained with indicated antibodies (as listed in Table S7).

Cytoplasmic and nuclear fractionation

The FACS-purified LPMs were resuspended in 150 μL of ice-cold lysis buffer (10 mM Tris-HCl, pH 7.5, 10 mM NaCl, 3 mM $MgCl_2$, 0.1% NP-40, 0.1% Tween-20, 0.01% Digitonin) and incubated on ice for 5 min with periodic vortexing. Then, add 1 mL of wash buffer (10mM Tris-HCl, pH 7.5, 10 mM NaCl, 3 mM $MgCl_2$, 0.1% Tween-20) and gently invert the tube for three times. Centrifuge the mixture at 500 × g for 10 min at 4°C. Collect the supernatant as the cytoplasmic fraction and wash the nuclei pellet with 1 mL PBS. Boil the cytoplasmic and nuclear protein with SDS sample loading buffer and proceed with immunoblotting analysis.

Purification and detection of ASC pyroptosome

ASC pyroptosome was purified using low-speed centrifugation and detected by disuccinimidyl suberate (DSS) cross-linking and subsequent immunoblotting for ASC oligomers as previously described.[129] Briefly, 4 million LPMs were pretreated with either vehicle or 30 μM BMS961 for 1 h and primed with 500 ng/mL LPS for 3 h, followed by 5 mM ATP stimulation for 30 min. Cells were washed once with ice-cold PBS and scraped off in 400 μL ice-cold lysis buffer (1% NP-40, 0.1 mM PMSF, cOmplete protease inhibitor in PBS). The cell lysate was fully disrupted by passing it through a 21-G needle for ten times on ice and then centrifuged at 250 × g for 5min at 4°C to remove the nucleus and cell debris. The protein concentration in each sample was quantified using the BCA protein assay. An equal amount of total protein was used to pellet the ASC pyroptosome by centrifuging at 5000 × g for 10 minat 4°C. The pellet was then resuspended in 300 μL of lysis buffer containing 2 mM fresh DSS and crosslinked for 30 min at room temperature. The reaction was quenched by adding 6 μL of 1 M Tris-HCl for 15 min. The cross-linked pellet was centrifuged at 5000 ×g for 5 min and resuspended in SDS sample loading buffer. Immunoblotting was performed to detect ASC oligomers in both soluble and pellet samples, with and without DSS crosslinking.

Statistical analyses

Statistical analyses, excluding the single-cell and population RNAseq data, were conducted using GraphPad Prism software. Data were shown as mean ± SD. Statistical significance was determined using two-tailed t test (paired or unpaired as indicated) for two groups, one-way ANOVA with Dunnett correction for three or more groups, and a Chi-square test for determining gene signature

significance in volcano plots. Additionally, a one-sample t-test with a hypothetical value of 1 was used for Figures 1B, 1D (top), and 1H. Statistical significance was defined as $P < 0.05$. The level of significance in all graphs is represented as follows: * for $P < 0.05$, ** for $P < 0.01$, *** for $P < 0.001$, and **** for $P < 0.0001$.

ACCESSION NUMBERS

GSE254573 is the umbrella accession number for these data.